Negative cell cycle regulation by Calcineurin is necessary for proper beta cell regeneration in zebrafish

Laura Massoz[1*], David Bergemann[1], Arnaud Lavergne[1,2], Célia Reynders[1], Caroline Désiront[1], Chiara Goossens[1], Lydie Flasse[1], Bernard Peers[1], Marianne L. Voz[1] and Isabelle Manfroid[1]

Author Affiliations

[1]Zebrafish Development and Disease Models laboratory, GIGA-Stem Cells, University of Liège, Liège, Belgium

[2]GIGA-Genomics core facility, GIGA, University of Liège, Liège, Belgium

*Corresponding author:

Email address: laura.massoz@doct.uliege.be

Abstract

Stimulation of pancreatic beta cell regeneration could be a therapeutic lead to treat diabetes. Unlike humans, the zebrafish can efficiently regenerate beta cells, notably from ductal pancreatic progenitors. To gain insight into the molecular pathways involved in this process, we established the transcriptomic profile of the ductal cells after beta cell ablation in the adult zebrafish. These data highlighted the protein phosphatase calcineurin as a new potential modulator of beta cell regeneration. We showed that calcineurin overexpression abolished the regenerative response, leading to glycemia dysregulation. On the opposite, calcineurin inhibition increased ductal cell proliferation and subsequent beta cell regeneration. Interestingly, the enhanced proliferation of the progenitors was paradoxically coupled with their exhaustion. This suggests that the proliferating progenitors are next entering in differentiation. Calcineurin appears as a guardian which prevents an excessive progenitor proliferation to preserve the pool of progenitors. Altogether, our findings reveal calcineurin as a key player in the balance between proliferation and differentiation to enable a proper beta cell regeneration.

Introduction

Blood glucose homeostasis is tightly controlled by pancreatic endocrine cells. Insulin-producing beta cells work in close association with alpha cells, which secrete glucagon, and delta cells secreting somatostatin, to maintain normal glycemia. The insulin plays a critical role in this process as it is the only hormone able to lower the glycemia. Beta cell loss is a hallmark of type 1 and of late stages of type 2 diabetes, leading to chronic hyperglycemia. Beta cell destruction is largely irreversible in human and in mammals, making the disease incurable nowadays. Nevertheless, studies in diabetic mice models uncovered promising evidences of slight recovery of beta cells via regeneration. For example, new beta cells can arise from the replication of remaining beta cells [1]. Different models of pancreas injuries revealed the plasticity of mammalian pancreatic cells. Actually, differentiated endocrine cells such as alpha cells[2] and delta cells[3] can reprogram and convert into insulin-producing cells, a process that is age dependent. Another possible source of beta cells could be de *novo* formation from pancreatic progenitors residing in the ductal compartment of the adult pancreas [4]. Lineage tracing experiments could not clearly highlight new beta cells arising from the ductal cells in the adult [4]–[6]. However, expression of the pro-endocrine marker Neurog3 was detected in the ducts in different mouse models of pancreas regeneration [4], [7], [8]. In addition, a rare population of ductal cells expressing Neurog3 has been reported to contribute to beta cell neogenesis during diabetes [9]. A recent study of single cell RNA sequencing reveal a sub-population of human ductal cells which are

able to give rise to all the pancreatic cell types, including beta cells, following implantation in mice [10]. Altogether, these findings suggest that mammalian pancreatic ducts possess the intrinsic capacity to (re)generate beta cells even though this process is poorly efficient and slow, especially in adults. In contrast to mammals, zebrafish possess remarkable capacity of regeneration, independently of its age [11]–[16]. This model can therefore be exploited to identify and characterize regenerative mechanisms and ultimately induce regeneration in mammals. Based on regenerative mechanisms identified in zebrafish, several studies succeed to improve regeneration in mammals, underlying the possibility of translation from zebrafish to mammals ([17]–[21] and [22], for review).

In zebrafish, the nitroreductase (NTR)/nitroaromatic prodrug system is widely used. In this technique, the combination of cell type-specific NTR expression and nitroaromatic prodrug exposure allow for controlled and targeted cell ablation [23], [24]. When NTR is expressed under the control of the *insulin* (*ins*) promoter (*Tg*(*ins:NTR-mCherry*) [25]), beta cell destruction is complete within 3 days following the treatment in adult fish, which correlate with a peak of hyperglycemia [26], [27]. The regeneration of beta cells upon ablation is spontaneous and fast and the glycemia is normalized within two weeks [13], [29]. Similar to mice, new beta cells can arise through proliferation of surviving beta cells [28] as well as through the contribution of alpha cells [29], [30] and delta cells[31], [32], underscoring the overall conservation of these processes from zebrafish to mammals. Nevertheless, unlike mammals, the presence of pancreatic progenitors in the ducts is well established in both larval [33] and adult zebrafish [26], [27]. Lineage tracing experiments pointed out that ductal cells and centroacinar cells (CACs) give rise to new beta cells [26], [33]. In adults, duct-derived beta cells start to be detected between 7 and 10 days following beta cell ablation [26], [27].

Notch signaling is a key player regulating the differentiation of duct-associated progenitors into endocrine cells. Larval duct cells as well as adult CACs display strong Notch activity [26], [34]. This signaling pathway has a central role in beta cell genesis during both development [35] and regeneration [33] by repressing endocrine differentiation. In zebrafish, different levels of Notch activity determine the behavior of the pancreatic progenitors. While a high level of Notch activity maintains cells in quiescence, a moderate level induces the entry in the cell cycle and proliferation whereas a low level drives endocrine differentiation of the progenitor cells [35]. A steep decrease of Notch activity pushes the progenitors to differentiate prematurely, bypassing the amplification step and leading to their depletion [35]. Repression of the Notch signaling by mTor, activated by glucose and nutrients, hence promotes beta cell formation and regeneration from ductal progenitors [33]. While Notch and mTor signaling are crucial for this process, there is still a need to establish a global view of the molecular mechanisms regulating beta cell regeneration.

93 To identify early events regulating ductal-derived beta cell regeneration, we determined the
94 transcriptomic signature of ductal cells from adult zebrafish following beta cell destruction. Our data
95 highlighted an upregulation of the Calcineurin (CaN) pathway. To elucidate CaN function in beta cell
96 regeneration, we both repressed and activated CaN pathway. We showed that CaN regulates beta cell
97 neogenesis in the ducts during regeneration, by acting on progenitor proliferation. Together, our
98 findings underline that CaN fine tunes the balance between progenitor proliferation and beta cell
99 differentiation to guarantee proper regeneration.

100

101 **Results**

102 *Transcriptomic profiling of ductal cells after beta cell destruction highlights regulation of calcineurin*
103 *pathway*

104 To gain a better understanding of the molecular mechanisms underlying the regeneration of beta cells
105 from the ducts, we determined the transcriptional landscape of ductal cells by RNA-sequencing after
106 beta cell ablation in the adult zebrafish. To selectively ablate the beta cells, we used the *Tg*(*ins:NTR-*
107 *mCherry*) transgenic fish. The ductal cells were labelled thanks to the *Tg*(*nkx6.1:GFP*) reporter line [27]
108 in which GFP marks the ductal tree and associated multipotent pancreatic progenitors [27]. More
109 precisely, 3 to 4 fishes were treated with the pro-drug MTZ at 10mM overnight, to induce ablation of
110 beta cells or with DMSO for the non-ablated controls. Ablation was confirmed by blood glucose
111 measurement before collection of the pancreas. To capture the early events triggered by the
112 destruction of beta cells, we generated the transcriptome of the ducts 3 days post ablation treatment
113 (dpt), *i.e.* before beta cell neogenesis (**Figure 1A supplemental**). Differential gene expression analysis
114 revealed that 1866 genes are up-regulated and 1515 genes down-regulated in the ductal cell of fish
115 treated with MTZ compared to control (pAdj < 0.05). According to Gene Ontology analysis, the most
116 enriched pathways among the up-regulated genes were DNA replication and cell cycle (**Figure 1A**). This
117 further corroborates our previous findings and those of others, regarding the activation of duct-
118 associated progenitors' proliferation in response to beta cell ablation [26], [27]. As expected, the Notch
119 pathway was enriched in the down-regulated genes [33], [35] (**Figure 1B**). On a contrasting note, in a
120 context marked by a robust proliferative response, we found it intriguing to observe an enrichment in
121 the cellular senescence signature (**Figure 1A**). Subsequently, we investigated deeper into the genes
122 associated with this specific signature. We found among them several components of the calcineurin
123 signaling pathway such as *nfatc3b*, *ppp3ccb* (the catalytic subunit of Calcineurin*), itpr2* and *calm3b*
124 **(Figure 1C)**. In addition to these genes related to the cellular senescence signature, our transcriptomic
125 studies revealed the modulation of other genes from the CaN canonical pathway (**Figure 1D**),
126 underlying its potential role in beta cell regeneration. Calcineurin (CaN) is a highly conserved

127 calcium/calmodulin dependent Ser/Thr phosphatase, involved in numerous biological process
128 including fin regeneration and beta cell function [36]–[39]. This prompted us to investigate the role of
129 CaN in beta cell regeneration.

130 Previous RNAseq data performed in our laboratory indicate that CaN (*ppp3cca/b*) and NFATc3
131 (*nfatc3a/b*) are mainly express in endocrine cells [40] (**Figure 1B supplemental**), which is in accordance
132 with the role of CaN/NFAT signalling in beta cells [41]. CaN genes (*ppp3cca/b*) as well as *nfatc3b,* are
133 express at lower levels in the ducts at basal state but their expression is induced in response to beta
134 cell destruction (**Figure 1C supplemental**).

135 *Calcineurin activity regulates the ductal regenerative response*

136 To evaluate the role of CaN in beta cell regeneration, more specifically derived from ductal progenitors,
137 we have chosen to use young larvae, where regenerated beta cells in the pancreatic tail arise
138 exclusively from the ducts [33]. In response to beta cells ablation, the intrapancreatic ducts undergo a
139 ductal regenerative response whereby differentiation toward the endocrine fate is increased [33]. We
140 first determined the rate of beta cell neogenesis from the ducts in response to a single acute ablation
141 of beta cells as we performed in adults. We treated *Tg*(*ins:NTR-P2A-mCherry*); *Tg*(*nkx6.1:GFP*) larvae
142 with nifurpirinol (NFP) from 3 to 4 dpf and mCherry+ beta cells were quantified in the GFP+ ducts in
143 the pancreatic tail at several time points: 4, 7, 10 and 14 dpt (**Figure 1E**). Duct-associated beta cells
144 started to be detected in non-ablated larvae between 7 and 10 dpt (**Figure 1F**) and the number of beta
145 cells slowly increased until 14 dpt (**Figure 1F, 1G**). In ablated larvae, the increase became more
146 pronounced from 10 dpt onwards (**Figure 1F, 1G**), indicating faster endocrine differentiation. This
147 experiment establishes that the ductal regenerative response is detectable between 10 and 14 days
148 after the beta cell ablation, performed at 3 dpf. We next wanted to determine if ductal cell proliferation
149 is activated in response to beta cell destruction in larvae as in adult fish. We exposed *Tg(ins:NTR-P2A-*
150 *mCherry); Tg(nkx6.1:GFP)* larvae to EdU the second day following ablation (**Figure 1H**). In the ablated
151 larvae, the proportion of GFP+ ductal cells EdU+ (in S-phase) was higher compared to non-ablated
152 larvae (**Figure 1I, 1J**). This result shows that acute beta cell ablation in larvae rapidly activates ductal
153 cell proliferation, as previously reported in adult zebrafish.

154 As our transcriptomic data from adult zebrafish revealed modulation of the CaN pathway at 3 dpt
155 (**Figure 1D**), we treated *Tg*(*ins:NTR-P2A-mCherry*); *Tg*(*nkx6.1:GFP*) larvae from 1 to 3 dpt after beta cell
156 ablation, with a CaN inhibitor, the Cyclosporin A (CsA) [39] (**Figure 2A**). The number of newly formed
157 beta cells in the tail was monitored from 4 to 14 dpt. CsA enhanced beta cell formation at 10 dpt (**Figure**
158 **2B-D)**. However, this effect appears to be transient since no discernible difference was observed
159 between the control and CsA-treated larvae in regeneration at the latest time point (14dpt), suggesting

160 an acceleration of the regenerative response (**Figure 2B, Figure 2A supplemental**). Interestingly, CsA
161 did not affect beta cell differentiation in non-ablated larvae, indicating that CsA only acts in a
162 regenerative context (**Figure 2B-D)**. Of note, CsA increased as well the number of regenerated beta
163 cells in the principal islet (**Figure 2B, 2C supplemental**). We and others, previously showed that the
164 other major source of beta cell regeneration, besides the ducts, are the bi-hormonal sst1.1+/ins+ cells
165 [31], [32], [42]. However, CsA did not affect bi-hormonal cell formation **(Figure 2D supplemental**),
166 suggesting that the additional cells in the principal islet could also originate from the ducts.

167 We next tested the effect of CsA on endocrine progenitors in a regenerative context. We induced
168 regeneration in Tg(*neurod1:GFP*) larvae where the GFP is expressed in both endocrine progenitors and
169 mature endocrine cells. We first assessed generation of GFP cells at different time points (**Figure 2E**
170 **supplemental)** and showed that CsA induced an increase of neurod1+ cells from 4 dpt. The increase
171 was still detectable at least until 10dpt (**Figure 2E, Figure 2F supplemental**). To determine if these
172 additional cells result from their own proliferation, we performed a pulse of EdU just before analysis
173 (**Figure 2E supplemental**). We observed that CsA did not affect the neurod1+ cell proliferation rate
174 ,which is very low at these stages (**Figure 2F**). As a consequence, the effect of CsA cannot be explained
175 by endocrine cell proliferation but rather by neogenesis from progenitors. As CsA affects pro-endocrine
176 cells formation, we next wondered if the increased cell formation induced by CsA is specific to beta
177 cells. Treatment with CsA was performed as previously and delta1.1 and alpha cells were detected by
178 immunofluorescence. Interestingly, CsA did not affect alpha nor delta1.1 cells neogenesis in response
179 to beta cell ablation (**Figure 2G-H supplemental**). Overall, these experiments showed that CsA affects
180 specifically the beta cells and their endocrine progenitors.

181 *CaN over-activation abolishes the regenerative response*

182 We then wondered if an opposite regulation of CaN *i.e.* its activation impacts as well the regenerative
183 response. To that end, we generated a transgenic line Tg(*hsp70:GFP-P2A-ppp3ccCA*) that allows
184 ubiquitous expression of a constitutively active form of CaN^{CA} (*ppp3cc*^{CA}) upon heat shocks. Beta cell
185 ablation was triggered in Tg(*hsp70:GFP-P2A-ppp3cc*^{CA}); Tg(*ins:NTR-P2A-mCherry*); Tg(*nkx6.1:GFP*)
186 larvae from 3 to 4 dpf and CaN^{CA} expression was induced by four successive heat-shocks from 1 to 3
187 dpt (**Figure 3A**). The overexpression of CaN^{CA} after ablation impaired the regenerative response at 14
188 dpt (**Figure 3B-C**). Similar results were obtained with Tg(*UAS:GFP-P2A-ppp3cc*^{CA}); Tg(*cftr:gal4*)[45] ;
189 Tg(*ins:NTR-P2A-mCherry*) larvae in which CaN^{CA} is continuously and specifically overexpressed in the
190 ducts within the pancreas (**Figure 3D-E**). Importantly, the structure of the ducts was similar in CaN^{CA}
191 overexpressing larvae compared to Tg(*nkx6.1:GFP*) controls (**Figure 3D**), suggesting that the
192 suppression of the regenerative response in CaN^{CA}-overexpressing larvae was not due to

193 morphogenetic defects during ductal growth. This result shows that CaN acts directly in the ducts to
194 decrease beta cell regeneration while it is not necessary for normal beta cell differentiation.

195 *CaN regulates beta cell differentiation induced by Notch inhibition in absence of regeneration*

196

197 Our transcriptomic data showed that the Notch pathway is downregulated in ductal cells during beta
198 cell regeneration (**Figure 1**). As the level of Notch activity determines the behavior of ductal cells [33]
199 from quiescence to proliferation and subsequently to beta cell differentiation, we tested whether
200 calcineurin acts together with the Notch pathway on a common pool of ductal progenitors. To inhibit
201 the Notch pathway, we treated larvae with several concentrations of the gamma-secretase inhibitor
202 LY411575 from 3 to 4dpf in absence of regeneration. The activity of CaN was inhibited by CsA during
203 the same timeframe (**Figure 4A**). As previously, we used reporter lines for beta and ductal cells
204 *Tg*(*ins:NTR-P2A-mCherry*); *Tg*(*nkx6.1:GFP*) and the number of secondary beta cells was analyzed at
205 6dpf (**Figure 4A**). As expected, the number of beta cells progressively rose as the concentration of the
206 Notch inhibitor increased (**Figure 4B**). Combined treatment with CsA fostered the differentiation of
207 beta cells between 1 and 10 µM LY411575 but did not result in further increase at 15 µM LY411575
208 (**Figure 4B**), suggesting that CaN is important within a permissive window of Notch activity. Since we
209 overserved the highest synergistic effect at 5µM of LY411575, we used this concentration for the
210 following experiments (**Figure 4C-D**). It is worth noting that combined treatment of LY411575 (5uM)
211 and another CaN inhibitor, FK506, resulted in the same synergistic increase of beta cell differentiation
212 (**Figure 4A-B supplemental**), confirming that the effect is well due to CaN inhibition. The combined
213 effect of Notch and CaN inhibition is transient as it is not observed at 7dpf anymore (**Figure 4E**).
214 Therefore, as observed in regenerative conditions (**Figure 2B**), CaN inhibition accelerates beta cell
215 neogenesis induced by Notch repression.

216 To determine to which extent CaN pathway can modulate Notch induced beta cell neogenesis, we
217 activated CaN^{CA} overexpression in *Tg*(*hsp70:GFP-P2A-ppp3cc*^{CA}*); Tg*(*ins:NTR-P2A-mCherry*) larvae by an
218 heat-shock at 3 dpf and treated them with LY411575 (**Figure 4C supplemental)**. CaN^{CA} overexpression
219 resulted in a lowered beta cell formation induced by Notch inhibition (**Figure 4D supplemental**),
220 revealing that CaN activation counterbalanced the effects of Notch inhibition. Using our previous
221 settings of Notch and CaN inhibition, we next wondered if the canonical pathway downstream of CaN
222 was involved in the enhancement of beta cell differentiation. To activate NFAT, a well-known target
223 of CaN, we used CHIR99021 allowing a stabilization of the active form of NFAT (**Figure 1D**). We found
224 that CHIR99021 rescued the effect of CsA (**Figure 4E supplemental**), suggesting that CaN inhibition
225 increases beta cell neogenesis at least partially by the regulation of NFAT. Overall, these results reveal
226 that CaN impacts beta cell formation in pro-endocrinogenic context, such as induced by a low level of

227 Notch activity. Moreover, it suggests that both CaN and Notch pathways act on a common pool of
228 ductal progenitors to govern beta cell neogenesis.

229

230 *CaN controls the proliferation of duct-associated progenitors induced by Notch inhibition*

231

232 Given that we observed the most significant increase in beta cell formation with CsA when Notch
233 activity was mildly repressed (**Figure 4B-D**), and since mild Notch activity has been shown to promote
234 progenitor amplification [35], it suggests that CaN acts at this level. To explore this possibility, we
235 exposed briefly *Tg*(*nkx6.1:GFP*) larvae to EdU after mild Notch (LY411575 5µM) and CaN inhibition
236 (**Figure 5A**) and analyzed at 4dpf and 6dpf. As expected, Notch inhibition increased the proportion of
237 proliferating EdU+ GFP+ ductal cells at 4dpf (**Figure 5B-C**) while the number of GFP+ ductal cells
238 remained constant (**Figure 5A supplemental**). Furthermore, the amount of ductal progenitors
239 decreased 2 days later (at 6dpf) (**Figure 5D**), which is concomitant with the increase of beta cell
240 differentiation (**Figure 4C-D**). Interestingly, the combined inhibition with CsA further increased these
241 proportions, while CaN inhibition alone had no effect (**Figure 5B-D**). Of note, we detected beta cells
242 EdU+ at 6dpf (**Figure 5B supplemental**), underlying that these cells originate from the proliferation of
243 ductal progenitors.

244 Incidentally, at 4dpf, while the proliferation is increased (**Figure 5C**), the number of ductal cells
245 remained the same in all conditions (**Figure 5A supplemental**), suggesting that ductal cells have not
246 yet left the cell cycle to differentiate. In comparison, after stronger Notch inhibition (15µM), the ductal
247 cells are already depleted at 4dpf (**Figure 5C supplemental**), as they directly differentiate without
248 entering the cell cycle [35]. In these conditions, CsA could therefore not enhance ductal progenitor
249 proliferation and thus beta cell formation (**Figure 4B**). These results show that CaN and Notch
250 pathways act together on the proliferation of the ductal progenitors to prevent their exhaustion.

251 *CaN prevents exhaustion of Notch responsive progenitors during beta cell regeneration*

252

253 Taken together, our results indicate that CaN plays a role in the proliferation of ductal progenitors in
254 contexts that are permissive for beta cell differentiation. To demonstrate that CaN acts on ductal
255 progenitor proliferation in a similar manner to Notch inhibition but during regeneration, we exposed
256 *Tg(ins:NTR-P2A-mCherry)*; *Tg(nkx6.1:GFP)* larvae after ablation and CsA treatment (**Figure 5E**). CaN
257 inhibition enhanced the proliferation of ductal cells in ablated larvae (**Figure 5F-G**). To next determine
258 if CaN acts on the Notch-responsive progenitors in beta cell regeneration, we then used

259 *Tg(tp1:VenusPest)* Notch reporter line. At larval stages the vast majority of ductal cells are Notch
260 responsive and the reporter line marks all the progenitors within the ductal tree [34]. We treated
261 *Tg(ins:NTR-P2A-mCherry*); *Tg(tp1:VenusPest)* as described above (**Figure 5E**). In ablated-larvae, CsA
262 increased tp1+ ductal cell proliferation (**Figure 5H-I**). Moreover, CsA induced a reduction of tp1+ ductal
263 cells in ablated larvae (**Figure 5 H-J**), suggesting an exhaustion of the Notch responsive progenitors, in
264 accordance with premature beta cell differentiation we observed (**Figure 2B-4D**). Lastly, CsA does not
265 affect tp1+ cells in non-ablated larvae showing that CaN inhibition did not directly affect Notch
266 signaling (**Figure 5J**). Those results suggest that CaN fine tunes the balance between proliferation of
267 the progenitors and their differentiation to prevent their exhaustion during beta cell regeneration.

268 *CaN regulation is functionally relevant in adult zebrafish*

269 To further expand upon our findings and investigate their relevance in a non-developmental context,
270 we next ought to determine whether CaN function is maintained in older zebrafish. We used 2 months
271 old *Tg*(*ins:NTR-P2A-mCherry*); *Tg*(*nkx6.1:GFP*) juveniles fish to perform beta cell ablation followed by
272 CsA treatments. We analyzed the number of small islets (up to 5 cells) at 7 and 10dpt. At 7dpt, CsA
273 increased the number of small islets in ablated juveniles (**Figure 6A-B**) showing that CaN inhibition
274 enhances beta cell regeneration in juvenile zebrafish, as in larvae. It is noteworthy that, as in larvae,
275 we highlighted an acceleration of beta cell regeneration. The increase number of small islets is indeed
276 transient as it not observe anymore at 10dpt (**Figure 6C**).

277 Next, we determined the functional impact of CaN overexpression or inhibition by assessing the
278 glycemia at 7, 10 and 14 after beta cell ablation. Overexpression of CaN^{CA} using either *Tg(hsp70:GFP-*
279 *P2A-ppp3cc*^{CA}*)* or *Tg*(*cftr:gal4*); *Tg*(*UAS:GFP-P2A-ppp3cc*^{CA}*),* led to an increased glycemia at both 7 and
280 10dpt (**Figure 6D-E)***,* before recovery at 14 dpt (**Figure 6A supplemental**). This indicates that the
281 overexpression of CaN delayed glycemia recovery induced by beta cell regeneration. However, CaN
282 inhibition did not seem to further improve the glycemia (**Figure 6D-E**) probably because the glycemia
283 was already low at 7dpt (77 mg/dL on average) compared to non-ablated control (50 mg/dl on average)
284 (**Figure 6D-E**). Altogether, these results show that in adult zebrafish also, CaN regulation is necessary
285 to enable beta cell regeneration and for proper recovery of the glycemia after beta cell loss.

286 **Discussion**

287 Previous drug and genetic screening using zebrafish larvae enabled the identification of several
288 regulators of beta cell regeneration from different pancreatic cellular sources. For example, adenosine
289 has been shown to stimulate beta cell replication [28], igfbp1a [43] and TGFb suppression [30] promote
290 alpha-to-beta cell transdifferentiation. As for cdk5 inhibition and folinic acid/Folr1, they promote beta
291 cell regeneration from the pancreatic ducts [44], [45]. Here, to identify novel regulators of beta cell

292 regeneration specifically from pancreatic ducts, we carried out a transcriptomic profiling of duct cells
293 following beta cell ablation in the adult zebrafish. Transcriptomic analyses show that the regulated
294 genes encompass most of the genes and pathways identified in previous studies (igfbp1, mTor, Notch,
295 etc.), underlying the importance of those actors in beta cell regeneration. Our data reveal also that
296 DNA replication is the most enriched signature attesting that duct cells undergo a potent proliferative
297 response after the destruction of beta cells.

298 Besides these expected signatures, our transcriptomic data uncover the unanticipated upregulation of
299 numerous genes implicated in DNA repair and cell cycle arrest. These signatures might indicate that
300 highly proliferating ductal cells activate counteracting mechanisms. Among the genes regulated in
301 those signatures, we focused on CaN and determined its role in beta cell regeneration. In an
302 experimental setting in the young larvae revealing regeneration from the ducts [33], pharmacological
303 inhibition of CaN increases the proliferation of duct cells induced by beta cell ablation, resulting in an
304 acceleration of beta cell regeneration in the ducts. Consistently, we also used a genetic approach, and
305 showed that transgene-mediated CaN overactivation abolishes the regenerative response.
306 Importantly, the inhibition of regeneration is observed when CaN is overexpressed either ubiquitously
307 or selectively in *cftr*-expressing ductal cells indicating that the role of CaN in beta cell regeneration is
308 intrinsic to the ducts. Moreover, we showed that CaN acts on the same pool of ductal progenitors than
309 Notch pathway and together control their proliferation and differentiation to beta cells. Altogether,
310 these experiments confirm that the increased of beta cells induced by CaN originate from the ducts in
311 the pancreatic tail. Nonetheless, while these experiments provide strong evidences, performing
312 lineage tracing would further reinforce these data. We also suggest that CaN could improve
313 regeneration in the principal islet, however as the molecular mechanisms of regeneration from the
314 extra pancreatic ducts are not Notch dependant, it would be interesting to investigate the mechanisms
315 under CaN inhibition.

316 Based on functional assays in larvae, we not only confirm the activation of the proliferation of ductal
317 cells soon after beta cell ablation, but also that the rate of progenitor proliferation is carefully
318 controlled by CaN in order to achieve proper and timely regeneration of beta cells. Our data are
319 consistent with earlier studies reporting a role of CaN in proliferation dynamics during fin regeneration.
320 In the regenerating fin, low CaN activity is found in the proximal region of the blastema characterized
321 by a high rate of proliferation and regeneration and its activity increases distally where lower
322 proliferation is observed [36], [38], [39]. It was suggested that CaN control blastemal cell progeny
323 divisions [36]. In human, the importance of CaN in proliferation is also highlighted in organ
324 transplanted patients. When patients are treated with Cyclosporin A (*i.e.* the CaN inhibitor we used in

325 this study) as immunosuppressive drug they indeed present an increased risk of skin cancer, notably
326 due to keratinocyte senescence inhibition [46].

327 It has been shown that Notch inhibitory treatments switch progenitors from proliferative self-renewing
328 to premature differentiation, leading to progenitor depletion [34], [35]. Our study reveals that this
329 phenomenon is further exacerbated by CaN inhibition. Importantly, during normal larval development
330 in absence of Notch inhibitory treatment, CaN does not affect basal ductal proliferation nor beta cell
331 differentiation. Hence, Notch signalling has to be repressed to detect the effect of CaN on the
332 progenitors, suggesting that CaN acts downstream of Notch pathway. In differentiating keratinocytes,
333 CaN cooperates with Notch signalling to regulate p21/*cdkn1a* (which is upregulated in the ducts at 3
334 dpt), cell cycle withdrawal and differentiation [47]. These studies show that CaN acts in association
335 with Notch signalling on progenitors proliferation and on their differentiation.

336 Based on our data, we build the model depicted in **Figure 7A**. Our study suggests that CaN acts in
337 competent progenitor cells and that this competence is determined by Notch signalling. When Notch
338 is repressed to a mild level, the progenitor enter into the cell cycle and acquire a pro-endocrinogenic
339 competence [35]. CaN acts on these progenitors to tone down an excessive proliferation and avoid the
340 exhaustion of these progenitors. CaN is therefore a guardian of the progenitor population. CaN
341 inhibition both increases progenitor proliferation and induces their depletion, suggesting a switch to a
342 symmetric division resulting in two daughter cells entering in endocrine differentiation.

343 More precisely, a previous study in mice uncover the existence of three division modes of the
344 pancreatic progenitors during embryonic development, *i.e.* symmetric self-renewing resulting in two
345 progenitors cells ; asymmetric resulting in a progenitor and a endocrine cell and symmetric
346 differentiative resulting in two differentiated cells [48]. The authors actually show that the type of
347 division is defined by the timing of induction of endocrine program by NEUROG3 [48]. Interestingly,
348 NEUROG3 seems to be the link between proliferation and differentiation, and its expression is
349 regulated by Notch signalling [49]. In zebrafish, endocrine differentiation is not induced by *Neurog3*
350 but by *Ascl1b* and *Neurod1* [50]. Concerning that subject, CaN inhibition accelerates the formation of
351 neurod1+ cells. Hence CaN could possibly act via the determination of the type of division *i.e.*
352 symmetric vs asymmetric. This model is supported by previous observation in others systems. In stem
353 cells and neuronal and hematopoietic progenitors, premature differentiation results from a switch in
354 the mode of cellular division, from symmetric amplifying division to asymmetric differentiating division
355 [51], [52]. Notch determines the choice between both types of divisions [53], [54].

356 Calcineurin is known to be implicated in cellular senescence [46]. Usually thought as negative
357 regulators of development and cellular growth, DNA repair [55] and cellular senescence [56] appear

358 to be required in both developmental and regenerative processes. Our transcriptomic data suggest
359 that these mechanisms are required for beta cell regeneration. Therefore, it would be interesting to
360 determine the contribution of these cellular processes in the ductal progenitors and determine if CaN
361 acts via cellular senescence in this case.

362 Overall, this study brings new insights on beta cell regeneration and highlights the ductal progenitor
363 cell cycle as a cornerstone in the process. Some studies report an increase of proliferation of some
364 ductal cell population in diabetic patients [10], [57], implying a regenerative response. However, these
365 ductal cells cannot efficiently reform the beta cell mass, suggesting a dormant mechanism of
366 regeneration. As such, the balance between proliferation and induction of endocrine differentiation
367 could be a key to improve beta cell neogenesis. However, as CaN is also important for beta cell
368 function, this approach would require to be transient to induce neogenesis. Therefore, it should be
369 combined with methods to induce beta cell proliferation to ultimately reconstitute the beta cell mass.
370 Overall, this study brings a better understanding on the regulation of the balance between ductal
371 progenitors proliferation and endocrine differentiation. These results should provide new hints to help
372 improve regenerative competences in mammals.

373

374 **Material and Methods**

375 *Key resources table*

Reagent type or resource	Designation	Source or reference	Identifier	Additional information
Genetic reagent (Danio rerio)	*TgBAC(nkx6.1:eGFP)^{ulg004}*	PMID: 26329351	ZFIN: ZDB-ALT-160205-1	
Genetic reagent (Danio rerio)	*Tg(ins:NTR-P2A-mCherry)^{ulg034}*	PMID: 29663654	ZFIN: ZDB-ALT-171122-9	
Genetic reagent (Danio rerio)	*Tg(cftr:gal4)*	PMID: 25592226	ZFIN : ZDB-FISH-150901-25442	
Genetic reagent (Danio rerio)	*Tg(tp1:VenusPest)*	PMID: 22492351	ZFIN: ZDB-FISH-150901-8023	
Genetic reagent (Danio rerio)	*Tg(hsp70:eGFP-P2A-ppp3ccaCA)^{ulg068}*	This paper		See Zebrafish husbandry and generation of the *Tg(hsp70:eGFP-P2A-*

				ppp3ccaCA) zebrafish line
Genetic reagent (Danio rerio)	*Tg(UAS:eGFP-P2A-ppp3ccaCA)* ^{ulg069}	This paper		See Zebrafish husbandry and generation of the *Tg(UAS:eGFP-P2A-ppp3ccaCA) zebrafish line*
Antibody	Anti-GFP (chicken polyclonal)	Aves Labs	GFP-1020	1:1000
Antibody	anti-mCherry/dsRed (Living Colors Polyclonal)	Clontech	632496	1:500
Antibody	Anti-glucagon (mouse polyclonal)	Sigma	G2654	1:300
Antibody	Goat anti-Chicken IgY (H+L), Alexa Fluor™ 488	Invitrogen	A-11039	1:750
Antibody	Goat anti-dsred 568	Invitrogen		1:750
Antibody	Goat anti-Mouse IgG (H+L) Cross-Adsorbed Secondary Antibody, Alexa Fluor 633	Invitrogen		1:750
Chemical compound	Nifurpirinol (NFP)	Sigma-Aldrich	32439	
Chemical compound	Metronidazole (MTZ)	Sigma-Aldrich	M1547	
Chemical compound	Cyclosporine A (CsA)	Selleckchem	S2286	
Chemical compound	LY411575	Sigma-Aldrich	SML0506	
Chemical compound	CHIR990211	Sellekchem	CT99021	
Commercial assay or kit	Gateway™ LR Clonase™ II Enzyme mix	Invitrogen	11791020	
Commercial assay or kit	Gateway™ BP Clonase™ II Enzyme mix	Invitrogen	11789020	
Sequence based reagent	IM369	This paper	PCR primer	gaagaaaaccccggtcctatgtcgacgaaagagccgaaag
Sequence based reagent	IM380	This paper	PCR primer	ccttacacattcccgtcagtgc
Sequence based reagent	IM371	This paper	PCR primer	CGGCTCTTTCGTCGACATAGGACCGGGGTTTTCTTCCACG
Sequence based reagent	O226	This paper	PCR primer	GCCACCATGGTGAGCAAGGGCGAGGA
Sequence based reagent	IM370	This paper	PCR primer	ttattagatcttatttctgatcacctccttt

Sequence based reagent	IM459	This paper	PCR primer	cacacgaattcgccgccaccATGGTGAGCAAGGGCGAG
Sequence based reagent	IM460	This paper	PCR primer	ggatcggtcgagatccttacGATCTTATTTCTGATCACCTCCTTACG
Sequence based reagent	IM457	This paper	PCR primer	GTAAGGATCTCGACCGATCCTG
Sequence based reagent	IM458	This paper	PCR primer	GGTGGCGGCGAATTCGTG
Commercial assay or kit	Nextera® XT DNA Library kit	Illumina	FC-131-1024	
Commercial assay or kit	Click-iT™ EdU Cell Proliferation Kit for Imaging, Alexa Fluor™ 647 dye	Invitrogen	C10340	
Software, algorithm	Imaris	Bitplane (http://www.bitplane.com/imaris/imaris)	RRID:SCR_007370	Version 9.5
Software, algorithm	GraphPad Prism	GraphPad Prism (https://graphpad.com)	RRID:SCR_015807	Version 8
Software, algorithm	DESeq2	DESeq2 (https://bioconductor.org/packages/release/bioc/html/DESeq2.html)	RRID:SCR_015687	
Software, algorithm	WebGestalt	WebGestalt (http://www.webgestalt.org/)	RRID:SCR_006786	

Zebrafish husbandry and generation of the Tg(hsp70:eGFP-P2A-ppp3ccaCA)^{ulg068} and Tg(UAS:eGFP-P2A-ppp2ccaCA)^{ulg069} zebrafish lines

Tg BAC(nkx6.1:eGFP)^{ulg004} [58] ; *Tg(ins:NTR-P2A-mCherry)^{ulg034}* [59] ; *Tg(cftr:gal4)* and *Tg(tp1:VenusPest)* were used. Zebrafish were raised in standard conditions at 28°C. All experiments were carried out in compliance with the European Union and Belgian law and with the approval of the ULiège Ethical Committee for experiments with laboratory animals (approval number : 2075).

The *hsp70:GFP-P2A-ppp3ccaCA* transgene has been generated by cloning a PCR fragment containing the Gateway vector pCR8/GW/TOPO. Firstly, we amplified the full length of ppp3ccaCA with primers

386 IM369/IM380 and amplified *GFP-P2A* with overlapping regions with IM371/O226. The overlapping PCR
387 used the primers O226/IM380. Then to obtain a truncated *ppp3ccaCA* lacking the calmodulin biding
388 and the autoinhibitory domain, resulting in a constantly active form of calcineurin, we amplified the
389 last fragments with IM370/O226 and cloned into PCR8 vector. The promoter was assembled by LR
390 recombination with pE5-hsp70 into pDestTol2p2A from the Tol2kit [60]. *Tg (hsp70:GFP-P2A-*
391 *ppp3ccaCA)* fish have been generated using the Tol2 mediated transgenesis [61]. *The Tg(UAS:GFP-*
392 *P2A-ppp3ccacA*) has been generated by ligation (KLD kit, NEB) of PCR fragments *GFP-P2A-ppp3ccacA*
393 *(*IM459/IM460) with the UAS sequences (IM457/IM458) in plasmid from (Distel 2009) and then
394 inserted into pDestTol2p2A from the Tol2kit. Final constructions has been injected with transposase
395 into wild type (WT) AB embryos.
396
397 *Beta-cell ablation*

398 Adults fish for RNA-sequencing experiment were treated with freshly prepared metronidazole (MTZ)
399 (Sigma M1547) at 10mM with 0.2% DMSO in fish water. Control treatments consisted of fish water
400 containing 0.2% DMSO. Fish were treated for 18 hours in the dark. Nifurpirinol (NFP) (32439, Sigma-
401 Aldrich) stock solution was dissolved at 2.5 mM in DMSO. b-cell ablation in *Tg(nkx6.1:eGFP);*
402 *Tg(ins:NTR-P2A-mCherry)* larvae was induced by treatment with 2.5 µM NFP in E3. Control treatments
403 consisted of E3 containing 0.2% DMSO. Larvae were treated for 18 hours in the dark.

404 *Drug treatments*

405 Cyclosporine A (Selleckchem, S2286), CHIR99021 and LY411575 (Sigma-Aldrich, SML0506) stock
406 solution were dissolved at 10mM in DMSO. Larvae treatment were respectively performed at 0.1 µM
407 and 5µM in E3. Control treatments consisted of E3 containing the same amount of DMSO than drug
408 treatment. Larvae were treated for 18 hours in the dark.

409 *5-ethynyl-2'-deoxyuridine (EdU) incorporation assay*

410 Zebrafish larvae were incubated in 4 mM EdU dissolved in E3 water for 8 hours, they were then directly
411 euthanised in tricaine and fixed in 4% PFA. EdU was detected according to the protocol of Click-iT™
412 EdU Cell Proliferation Kit for Imaging, Alexa Fluor™ 647 (ThermoFisher C10340) after whole mount
413 immunodetection.

414 *Heat Shock*

415 *Successive heat shocks of 30 minutes and 12 hours apart were performed at 39°C for larvae and 37°C*
416 *for juveniles and adults zebrafish.*

417 *Whole mount immunodetection*

418 Larvae were euthanized in tricaine and fixed in 4% PFA at 4 °C for IHC. The digestive tract of juveniles
419 was dissected prior immunodetection and kept in methanol for at least 18 hours. After depigmentation
420 with 3% H2O2/1% KOH, larvae were permeabilised 30 min in PBS/ Triton X-100 and incubated for two
421 hours in blocking buffer (4% goat serum/1% BSA/PBS/0.1% Triton X-100). Primary and secondary
422 antibodies were incubated at 4 °C overnight.

	Fixation duration	Depigmentation duration	Permeabilization solution	Permeabilization duration
5-10 dpf	18 hours	15 min	PBTr 0.05%	30 min
13-17 dpf	36 hours	20 min	PBTr 2%	30 min
2months (digestive tract)	18 hours	15 min	/	/

423

424 Primary antibodies: Living Colors Polyclonal anti-mCherry/dsRed (rabbit, 1:500, Clontech 632496),
425 anti-GFP (chicken, 1:1000),

426 Secondary antibodies: Alexa Fluor-488, -568, -633 (goat, 1:750, Molecular Probes).

427 *Flow cytometry and FACS*

428 The whole pancreas from 3-4 fish of *Tg(nkx6.1:eGFP); Tg(ins:NTR-P2A-mCherry)* adult fish (6–10
429 months old, males and females) were dissected, collected and washed in HBSS without Ca^{2+}/Mg^{2+}. Live
430 cell dissociation was performed in Tryple Select 1x solution (GIBCO) supplemented with 100 U/mL
431 collagenase IV (Life Technologies 17104-019) and 40 µg/mL proteinase K (Invitrogen, 25530031) for 10
432 min at 28 °C.

433 The GFP+ cells were selected on FACS Aria III and sorted under purity mode and after exclusion of the
434 doublets. The purity of the sorted cells was confirmed by epifluorescence microscopy (~95 %). Cells
435 (about 1000-5000/fish depending on the cell type) were immediately lysed with 0.5% Triton X-100
436 containing 2U/µl RNAse inhibitor and stored at –80 °C.

437 *mRNA sequencing of FACSed cells and bioinformatic analyses*

438 cDNAs were prepared from lysed cells according to SMART-Seq2.0 (Picelli et al., 2014) for low input
439 RNA sequencing and libraries were prepared with Nextera® DNA Library kit (Illumina). Independent
440 biological replicates of each cell type sequenced using Illumina NextSeq500 and obtained ~20 million
441 100 bp paired-end reads. Reads were mapped and aligned to the zebrafish genome GRCz11 from
442 Ensembl gene annotation version using STAR version 2.6.1 (Dobin et al., 2013). Gene expression levels
443 were calculated with featureCounts (http://bioinf.wehi.edu.au/featureCounts/) and differential
444 expression determined with DESeq2 (Love, Huber, & Anders, 2014). Expression values are given as
445 normalized read counts. Poorly expressed genes with mean normalized expression counts <10 were
446 excluded from the subsequent analyses. DESeq2 uses Wald test for significance with posterior
447 adjustment of P values (Padj) using Benjamini and Hochberg multiple testing. The differentially
448 expressed (DE) genes identified with a Padj cutoff of 0.05 were submitted for GO analysis using
449 WebGestalt tool (Liao, Wang, Jaehnig, Shi, &Zhang, 2019).

450 *Confocal microscopy and image analysis*

451 Images were acquired using Leica SP5 confocal microscope. We used ImageJ to count the cells and
452 Imaris to do the pictures.

453 *Glycemia measurement*

454 *Glycemia measurement were performed as described in* [59].

455 **Data availability**

456 The sequences that support the findings are of this study have been deposit in Geo with the accessions
457 codes GSE212124, https://www.ncbi.nlm.nih.gov/geo/info/linking.html. The authors declare that all
458 other data supporting the findings of this study are available within the paper and its supplementary
459 information files.

460 **Authors contribution**

461 **L.M.** conducted experiments, acquired and analysed data, analysed transcriptomic data, wrote the
462 manuscript. **D.B.** conducted RNA-seq experiment and revised the manuscript **A.L.** implemented
463 bioinformatic programs and analysed transcriptomic data. **C.R., C.G. and C.D.** conducted experiments.
464 **L.F.** revised the manuscript. **B.P.** provided resources and advised on research studies. **M.L.V.** provided
465 resources, advised on research studies and revised the manuscript **I.M.** supervised the whole work,
466 acquired funding, designed the research studies, verified data and assisted in writing the manuscript.

467 **Acknowledgments**

468 The authors thank the EOS (Excellence of Sciences) program from FNRS and more especially Dr.
469 Emmanuel Dejardin for support. We also thank the GIGA technology platforms, GIGA-Genomics and
470 GIGA-Imaging. The authors also thanks Jérémie Zappia for critically reading the manuscript, Jordane
471 Bourdouxhe and Marie Alice Dupont for their help with the constructions.

472 **Duality of interest**

473 No potential conflicts of interest.

474 **References**

475 [1] Y. Dor, J. Brown, O. I. Martinez, and D. a Melton, "Adult pancreatic beta-cells are formed by
476 self-duplication rather than stem-cell differentiation.," *Nature*, vol. 429, no. model 3, pp. 41–
477 46, 2004, doi: 10.1038/nature02520.

478 [2] F. Thorel *et al.*, “Conversion of Adult Pancreatic alpha-cells to Beta-cells after Extreme Beta
479 Cell Loss,” *Nature*, vol. 464, no. 7292, pp. 1149–1154, 2010, doi:
480 10.1038/nature08894.Conversion.

481 [3] S. Chera *et al.*, “Diabetes recovery by age-dependant conversion of pancreatic delta-cells into
482 insulin producers,” *Nature*, vol. 514, no. 7523, pp. 503–507, 2014, doi:
483 10.1038/nature13633.Diabetes.

484 [4] X. Xu *et al.*, “Beta Cells Can Be Generated from Endogenous Progenitors in Injured Adult
485 Mouse Pancreas,” *Cell*, vol. 132, pp. 197–207, 2008, doi: 10.1016/j.cell.2007.12.015.

486 [5] M. Solar *et al.*, “Pancreatic Exocrine Duct Cells Give Rise to Insulin-Producing β Cells during
487 Embryogenesis but Not after Birth,” *Dev. Cell*, vol. 17, pp. 849–860, 2009, doi:
488 10.1016/j.devcel.2009.11.003.

489 [6] H. Zhao *et al.*, “Pre-existing beta cells but not progenitors contribute to new beta cells in the
490 adult pancreas,” *Nat. Metab.*, vol. 3, no. 3, pp. 352–365, 2021, doi: 10.1038/s42255-021-
491 00364-0.

492 [7] J. L. Kopp *et al.*, “Sox9+ ductal cells are multipotent progenitors throughout development but
493 do not produce new endocrine cells in the normal or injured adult pancreas,” *Development*,
494 vol. 138, pp. 653–665, 2011, doi: 138/4/653 [pii].

495 [8] M. Courtney *et al.*, “The Inactivation of Arx in Pancreatic α-Cells Triggers Their Neogenesis and
496 Conversion into Functional β-Like Cells,” *PLoS Genet.*, vol. 9, no. 10, pp. 1–18, 2013, doi:
497 10.1371/journal.pgen.1003934.

498 [9] C. Gribben *et al.*, “Ductal Ngn3-expressing progenitors contribute to adult β cell neogenesis in
499 the pancreas,” *Cell Stem Cell*, vol. 28, no. 11, pp. 2000-2008.e4, 2021, doi:
500 10.1016/j.stem.2021.08.003.

501 [10] M. M. F. Qadir *et al.*, “Single-cell resolution analysis of the human pancreatic ductal
502 progenitor cell niche,” *Proc. Natl. Acad. Sci. U. S. A.*, vol. 117, no. 20, pp. 10876–10887, 2020,
503 doi: 10.1073/pnas.1918314117.

504 [11] J. B. Moss, P. Koustubhan, M. Greenman, M. J. Parsons, I. Walter, and L. G. Moss,
505 “Regeneration of the pancreas in adult zebrafish,” *Diabetes*, vol. 58, no. August, pp. 1844–
506 1851, 2009, doi: 10.2337/db08-0628.

507 [12] K. D. Poss, L. G. Wilson, and M. T. Keating, “Heart regeneration in zebrafish,” *Science (80-.).*,
508 vol. 298, no. 5601, pp. 2188–2190, 2002, doi: 10.1126/science.1077857.

509 [13] T. Y. Choi, N. Ninov, D. Y. R. Stainier, and D. Shin, “Extensive conversion of hepatic biliary
510 epithelial cells to hepatocytes after near total loss of hepatocytes in zebrafish,”
511 *Gastroenterology*, vol. 146, no. 3, pp. 776–788, 2014, doi: 10.1053/j.gastro.2013.10.019.

512 [14] Y. Goldshmit, T. E. Sztal, P. R. Jusuf, T. E. Hall, M. Nguyen-Chi, and P. D. Currie, “Fgf-dependent
513 glial cell bridges facilitate spinal cord regeneration in zebrafish.,” *J. Neurosci.*, vol. 32, no. 22,
514 pp. 7477–7492, May 2012, doi: 10.1523/JNEUROSCI.0758-12.2012.

515 [15] V. Kroehne, D. Freudenreich, S. Hans, J. Kaslin, and M. Brand, “Regeneration of the adult
516 zebrafish brain from neurogenic radial glia-type progenitors,” *Development*, vol. 138, no. 22,
517 pp. 4831–4841, 2011, doi: 10.1242/dev.072587.

518 [16] M. Gemberling, T. J. Bailey, D. R. Hyde, and K. D. Poss, “The zebrafish as a model for complex
519 tissue regeneration,” *Trends Genet.*, vol. 29, no. 11, pp. 611–620, 2013, doi:
520 10.1016/j.tig.2013.07.003.

521 [17] C. Papadimitriou *et al.*, “3D Culture Method for Alzheimer’s Disease Modeling Reveals
522 Interleukin-4 Rescues Aβ42-Induced Loss of Human Neural Stem Cell Plasticity,” *Dev. Cell*, vol.
523 46, no. 1, pp. 85-101.e8, 2018, doi: 10.1016/j.devcel.2018.06.005.

524 [18] V. Mashkaryan *et al.*, “Type 1 Interleukin-4 Signaling Obliterates Mouse Astroglia in vivo but
525 Not in vitro,” *Front. Cell Dev. Biol.*, vol. 8, no. February, pp. 1–16, 2020, doi:
526 10.3389/fcell.2020.00114.

527 [19] S. Ko, T. Choi, J. O. Russell, J. So, and D. Shin, “Bromodomain and extraterminal (BET) proteins
528 regulate biliary-driven liver regeneration,” *J. Hepatol.*, vol. 64, no. 2, pp. 316–325, 2016, doi:
529 10.1016/j.jhep.2015.10.017.Bromodomain.

530 [20] Y. Goldshmit *et al.*, “Decreased anti-regenerative effects after spinal cord injury in spry4-/-
531 mice.,” *Neuroscience*, vol. 287, pp. 104–112, Feb. 2015, doi:
532 10.1016/j.neuroscience.2014.12.020.

533 [21] B. V. Fausett, J. D. Gumerson, and D. Goldman, “The proneural basic helix-loop-helix gene
534 Ascl1a is required for retina regeneration,” *J. Neurosci.*, vol. 28, no. 5, pp. 1109–1117, 2008,
535 doi: 10.1523/JNEUROSCI.4853-07.2008.

536 [22] L. Massoz, M. A. Dupont, and I. Manfroid, “Zebra-fishing for regenerative awakening in
537 mammals,” *Biomedicines*, vol. 9, no. 1, pp. 1–18, 2021, doi: 10.3390/biomedicines9010065.

538 [23] H. Pisharath, “Validation of nitroreductase, a prodrug-activating enzyme, mediated cell death
539 in embryonic zebrafish (Danio rerio),” *Comp. Med.*, vol. 57, no. 3, pp. 241–246, 2007.

540 [24] S. Curado, R. M. Anderson, B. Jungblut, J. Mumm, E. Schroeter, and D. Y. R. Stainier,
541 "Conditional targeted cell ablation in zebrafish: A new tool for regeneration studies," *Dev.*
542 *Dyn.*, vol. 236, no. February, pp. 1025–1035, 2007, doi: 10.1002/dvdy.21100.

543 [25] H. Pisharath, J. M. Rhee, M. a Swanson, S. D. Leach, and M. J. Parsons, "Targeted ablation of
544 beta cells in the embryonic zebrafish pancreas using E.coli nitroreductase," *Mech Dev.*, 2007,
545 doi: 10.1016/j.mod.2006.11.005.Targeted.

546 [26] F. Delaspre *et al.*, "Centroacinar cells are progenitors that contribute to endocrine pancreas
547 regeneration," *Diabetes*, vol. 64, no. October, pp. 3499–3509, 2015, doi: 10.2337/db15-0153.

548 [27] A. P. Ghaye *et al.*, "Progenitor potential of nkx6.1-expressing cells throughout zebrafish life
549 and during beta cell regeneration," *BMC Biol.*, vol. 13, p. 70, 2015, doi: 10.1186/s12915-015-
550 0179-4.

551 [28] O. Andersson *et al.*, "Adenosine signaling promotes regeneration of pancreatic β- cells in
552 vivo," *Cell Metab.*, 2012, doi: 10.1016/j.cmet.2012.04.018.Adenosine.

553 [29] L. Ye, M. A. Robertson, D. Hesselson, D. Y. R. Stainier, and R. M. Anderson, "Glucagon is
554 essential for alpha cell transdifferentiation and beta cell neogenesis," *Dev.*, vol. 142, no. 8, pp.
555 1407–1417, 2015, doi: 10.1242/dev.117911.

556 [30] C. S. M. Helker *et al.*, "A whole organism small molecule screen identifies novel regulators of
557 pancreatic endocrine development," *Dev.*, vol. 146, no. 14, 2019, doi: 10.1242/dev.172569.

558 [31] C. Carril Pardo *et al.*, "A delta-cell subpopulation with a pro-beta-cell identity contributes to
559 efficient age-independent recovery in a zebrafish model of diabetes," *Elife*, 2022.

560 [32] S. P. Singh *et al.*, "A single-cell atlas of de novo β-cell regeneration reveals the contribution of
561 hybrid β/δ-cells to diabetes recovery in zebrafish," *Development*, vol. 149, no. 2, 2022, doi:
562 10.1242/dev.199853.

563 [33] N. Ninov, D. Hesselson, P. Gut, A. Zhou, K. Fidelin, and D. Y. R. Stainier, "Metabolic regulation
564 of cellular plasticity in the pancreas," *Curr. Biol.*, vol. 23, no. 13, pp. 1242–1250, 2013, doi:
565 10.1016/j.cub.2013.05.037.

566 [34] M. J. Parsons *et al.*, "Notch-responsive cells initiate the secondary transition in larval zebrafish
567 pancreas," *Mech. Dev.*, vol. 126, no. 10, pp. 898–912, 2009, doi: 10.1016/j.mod.2009.07.002.

568 [35] N. Ninov, M. Borius, and D. Y. R. Stainier, "Different levels of Notch signaling regulate
569 quiescence, renewal and differentiation in pancreatic endocrine progenitors," *Development*,

570 vol. 139, no. 9, pp. 1557–1567, 2012, doi: 10.1242/dev.076000.

571 [36] V. A. Tornini *et al.*, “Live Monitoring of Blastemal Cell Contributions During Appendage
572 Regeneration,” *Curr. Biol.*, 2016, doi: 10.1016/j.cub.2016.08.072.Live.

573 [37] S. C. McMillan *et al.*, “A regulatory pathway involving retinoic acid and calcineurin demarcates
574 and maintains joint cells and osteoblasts in regenerating fin,” *Dev.*, vol. 145, no. 11, 2018, doi:
575 10.1242/DEV.161158.

576 [38] Z. Cao *et al.*, “Calcineurin controls proximodistal blastema polarity in zebrafish fin
577 regeneration,” *Proc. Natl. Acad. Sci. U. S. A.*, vol. 118, no. 2, pp. 2–9, 2021, doi:
578 10.1073/pnas.2009539118.

579 [39] S. Kujawski *et al.*, “Calcineurin Regulates Coordinated Outgrowth of Zebrafish Regenerating
580 Fins,” *Dev. Cell*, vol. 28, no. 5, pp. 573–587, 2014, doi: 10.1016/j.devcel.2014.01.019.

581 [40] E. Tarifeño-Saldivia *et al.*, “Transcriptome analysis of pancreatic cells across distant species
582 highlights novel important regulator genes,” *BMC Biol.*, vol. 15, no. 1, pp. 1–19, 2017, doi:
583 10.1186/s12915-017-0362-x.

584 [41] J. J. Heit *et al.*, “Calcineurin/NFAT signalling regulates pancreatic β-cell growth and function,”
585 *Nature*, vol. 443, no. 7109, pp. 345–349, 2006, doi: 10.1038/nature05097.

586 [42] J. Mi, K. C. Liu, and O. Andersson, “Decoding pancreatic endocrine cell differentiation and β
587 cell regeneration in zebrafish,” *Sci. Adv.*, vol. 9, no. 33, p. eadf5142, 2023, doi:
588 10.1126/sciadv.adf5142.

589 [43] J. Lu *et al.*, “ IGFBP 1 increases β-cell regeneration by promoting α- to β-cell
590 transdifferentiation ,” *EMBO J.*, vol. 35, no. 18, pp. 2026–2044, 2016, doi:
591 10.15252/embj.201592903.

592 [44] C. Karampelias *et al.*, “Reinforcing one-carbon metabolism via folic acid/Folr1 promotes β-cell
593 differentiation,” *Nat. Commun.*, vol. 12, no. 1, pp. 1–13, 2021, doi: 10.1038/s41467-021-
594 23673-0.

595 [45] K. C. Liu *et al.*, “Inhibition of Cdk5 promotes β-cell differentiation from ductal progenitors,”
596 *Diabetes*, vol. 67, no. 1, pp. 58–70, 2017, doi: 10.2337/db16-1587.

597 [46] X. Wu *et al.*, “Calcineurin and ATF3: opposite roles in squamous skin cancer,” *Nature*, 2010,
598 doi: 10.1038/nature08996.Calcineurin.

599 [47] C. Mammucari *et al.*, “Integration of notch 1 and calcineurin/NFAT signaling pathways in

600 keratinocyte growth and differentiation control," *Dev. Cell*, vol. 8, no. 5, pp. 665–676, 2005,
601 doi: 10.1016/j.devcel.2005.02.016.

602 [48] Y. H. Kim, H. L. Larsen, P. Rué, L. A. Lemaire, J. Ferrer, and A. Grapin-Botton, "Cell Cycle–
603 Dependent Differentiation Dynamics Balances Growth and Endocrine Differentiation in the
604 Pancreas," *PLoS Biol.*, vol. 13, no. 3, 2015, doi: 10.1371/journal.pbio.1002111.

605 [49] N. A. J. Krentz *et al.*, "Phosphorylation of NEUROG3 Links Endocrine Differentiation to the Cell
606 Cycle in Pancreatic Article Phosphorylation of NEUROG3 Links Endocrine Differentiation to the
607 Cell Cycle in Pancreatic Progenitors," *Dev. Cell*, vol. 41, no. 2, pp. 129-142.e6, 2017, doi:
608 10.1016/j.devcel.2017.02.006.

609 [50] L. C. Flasse, D. G. Stern, J. L. Pirson, I. Manfroid, B. Peers, and M. L. Voz, "The bHLH
610 transcription factor Ascl1a is essential for the specification of the intestinal secretory cells and
611 mediates Notch signaling in the zebrafish intestine," *Dev. Biol.*, vol. 376, no. 2, pp. 187–197,
612 2013, doi: 10.1016/j.ydbio.2013.01.011.

613 [51] W. B. Huttner and Y. Kosodo, "Symmetric versus asymmetric cell division during neurogenesis
614 in the developing vertebrate central nervous system," *Curr. Opin. Cell Biol.*, vol. 17, no. 6, pp.
615 648–657, 2005, doi: 10.1016/j.ceb.2005.10.005.

616 [52] A. D. Ho and W. Wagner, "The beauty of asymmetry: Asymmetric divisions and self-renewal in
617 the haematopoietic system," *Curr. Opin. Hematol.*, vol. 14, no. 4, pp. 330–336, 2007, doi:
618 10.1097/MOH.0b013e3281900f12.

619 [53] R. S. Bultje, D. R. Castaneda-Castellanos, L. Y. Jan, Y. N. Jan, A. R. Kriegstein, and S. H. Shi,
620 "Mammalian Par3 Regulates Progenitor Cell Asymmetric Division via Notch Signaling in the
621 Developing Neocortex," *Neuron*, vol. 63, no. 2, pp. 189–202, 2009, doi:
622 10.1016/j.neuron.2009.07.004.

623 [54] M. Guo, L. Y. Jan, and Y. N. Jan, "Control of daughter cell fates during asymmetric division:
624 Interaction of Numb and Notch," *Neuron*, vol. 17, no. 1, pp. 27–41, 1996, doi: 10.1016/S0896-
625 6273(00)80278-0.

626 [55] K. Sousounis *et al.*, "Eya2 promotes cell cycle progression by regulating DNA damage response
627 during vertebrate limb regeneration," 2020.

628 [56] S. Da *et al.*, "Cell senescence contributes to tissue regeneration in zebrafish," no. July 2019,
629 pp. 1–5, 2020, doi: 10.1111/acel.13052.

630 [57] A. S. Md Moin, P. C. Butler, and A. E. Butler, "Increased proliferation of the pancreatic duct

631 gland compartment in type 1 diabetes," *J. Clin. Endocrinol. Metab.*, vol. 102, no. 1, pp. 200–
632 209, 2017, doi: 10.1210/jc.2016-3001.

633 [58] A. P. Ghaye *et al.*, "Progenitor potential of nkx6.1-expressing cells throughout zebrafish life
634 and during beta cell regeneration," *BMC Biol.*, vol. 13, no. 1, 2015, doi: 10.1186/s12915-015-
635 0179-4.

636 [59] D. Bergemann *et al.*, "Nifurpirinol: A more potent and reliable substrate compared to
637 metronidazole for nitroreductase-mediated cell ablations," *Wound Repair Regen.*, vol. 26, no.
638 2, pp. 238–244, 2018, doi: 10.1111/wrr.12633.

639 [60] K. M. Kwan *et al.*, "The Tol2kit: a multisite gateway-based construction kit for Tol2 transposon
640 transgenesis constructs.," *Dev. Dyn. an Off. Publ. Am. Assoc. Anat.*, vol. 236, no. 11, pp.
641 3088–3099, Nov. 2007, doi: 10.1002/dvdy.21343.

642 [61] K. Kawakami, "Tol2: a versatile gene transfer vector in vertebrates.," *Genome Biol.*, vol. 8
643 Suppl 1, p. S7, 2007, doi: 10.1186/gb-2007-8-s1-s7.

644

645 **Legends**

646

647 **Figure 1 :** *Transcriptomic profiling of ductal cells during beta cell regeneration and validation in larvae*

648 A-B) Enrichment ratio of selected non-redundant signatures of KEGG pathways overrepresented
649 in ductal cells after beta cells ablation (UP – A and DOWN -B) compared to ductal cells without
650 beta cells ablation. Gene Ontology (GO) terms were identified using ORA analysis by WebGestalt
651 (Liao et al., 2019) using the list of DE genes provided by DESeq. The light color for Notch pathway
652 means p-value = 0.11.

653 C) List of genes associated with the signature of cellular senescence from A-B. Genes related to
654 CaN pathway are in bold.

655 D) Calcineurin canonical pathway with up-regulated genes in green and down-regulated genes in
656 red in transcriptomic data from A-B.

657 E) Experimental design for regeneration test in larvae. Briefly, after nifurpirinol treatment from 3
658 to 4dpf, larvae were fixed and analyzed at 4-7-10 and 14 days post treatment (dpt).

659 F) Graph representing the mean number of mCherry+ beta cells in the pancreatic tail of *Tg(ins:NTR-*
660 *P2A-mCherry) ; Tg(nkx6.1:GFP)* at 0-4-7-10 and 14 dpt. The gray spheres represent non-ablated
661 conditions and the pink triangles the ablated condition. Data are presented as mean values ± SEM.
662 One-way ANOVA test with Tukey's multiple comparison test, ****p-value<0.0005.

663 G) Whole mount fluorescent immunohistochemistry (GFP and mCherry) of the pancreas of
664 *Tg(ins:NTR-P2A-mCherry) ; Tg(nkx6.1:GFP)* larvae at 14dpt. 3D projection (stack) of one non-

665 ablated and one ablated representative samples. The principal islet (PI) and the pancreatic tail are
666 shown. Arrows point out mCherry+ beta cells in the pancreatic tail. Scale 100µM.

667 H) Experimental design for EdU assay in larvae. After NFP treatment for 3 to 4dpf, larvae were
668 exposed to EdU at 2dpt before fixation for analysis.

669 I) Whole mount fluorescent immunohistochemistry (GFP and EdU) of the pancreatic tail of
670 *Tg(ins:NTR-P2A-mCherry) ; Tg(nkx6.1:GFP)* larvae at 2dpt. 3D projection (stack) of one non-ablated
671 and one ablated representative samples. Arrows point out GFP+ duct cells EdU+ in the pancreatic
672 tail. Scale 50µM.

673 J) Barplot representing the percentage of GFP+ ductal cells which incorporated EdU+ in non-
674 ablated and ablated conditions. Data are presented as mean values ± SD. T-test. **p-value<0.005.

675

676 **Figure 2 :** *Calcineurin inhibition with CsA increases the ductal regenerative response*

677 **A)** Experimental design for regeneration test in larvae with CsA treatment. Briefly, after
678 nifurpirinol treatment from 3 to 4dpf, larvae were treated with CsA from 1 to 3dpt and fixed
679 and analyzed at 4-7-10 and 14 days post treatment (dpt).
680 **B)** Graph representing the mean number of mCherry+ beta cells in the pancreatic tail of
681 *Tg(ins:NTR-P2A-mCherry) ; Tg(nkx6.1:GFP)* at 0-4-7-10 and 14 dpt. The gray spheres represent
682 non-ablated condition ; the pink triangles represent the ablated condition ; the black squares
683 CsA condition and inverted green triangles ablated + CsA condition. Data are presented as
684 mean values ± SEM. Two-way ANOVA test with Sidak's multiple comparisons test, *p-
685 value<0.05.
686 **C)** Whole mount fluorescent immunohistochemistry (GFP and mCherry) of the pancreas of
687 *Tg(ins:NTR-P2A-mCherry) ; Tg(nkx6.1:GFP)* larvae at 10dpt. 3D projection (stack) of non-
688 ablated and ablated larvae treated with DMSO or CsA representative samples. The principal
689 islet (PI) and the pancreatic tail are shown. Arrows point out mCherry+ beta cells in the
690 pancreatic tail. Scale 100µM.
691 **D)** Barplot representing the number of number of mCherry+ beta cells in the pancreatic tail of
692 *Tg(ins:NTR-P2A-mCherry) ; Tg(nkx6.1:GFP)* larvae at 10dpt. The gray spheres represent non-
693 ablated condition ; the pink triangles represent the ablated condition ; the black squares CsA
694 condition and inverted green triangles ablated + CsA condition. Data are presented as mean
695 values ± SD. Two-way ANOVA with Tukey's multiple comparison test, *p-value<0.05.
696 **E)** Graph representing the mean number of GFP+ neurod1+ cells in the pancreatic tail of
697 *Tg(ins:NTR-P2A-mCherry) ; Tg(neurod1:GFP)* at 0-4-7 and 10 dpt. The gray spheres represent
698 non-ablated condition ; the pink triangles represent the ablated condition ; the black squares
699 CsA condition and inverted green triangles ablated + CsA condition. Data are presented as
700 mean values ± SEM. Two-way ANOVA test with Sidak's multiple comparisons test, **p-
701 value<0.005; *** p-value<0.0005; **** p-value<0.00005.
702 **F)** Graph representing the mean number of GFP+ neurod1 EdU+ cells in the pancreatic tail of
703 *Tg(ins:NTR-P2A-mCherry) ; Tg(neurod1:GFP)* at 0-4-7 and 10 dpt. The gray spheres represent
704 non-ablated condition ; the pink triangles represent the ablated condition ; the black squares
705 CsA condition and inverted green triangles ablated + CsA condition. Data are presented as
706 mean values ± SEM.
707
708

709 **Figure 3:** *Transgenic mediated overexpression of calcineurin abolish the ductal regenerative response*
710

711 **A)** Experimental design for regeneration test in larvae with heat-shocks. Briefly, after nifurpirinol
712 treatment from 3 to 4dpf, four heat shock were performed from 1 to 3dpt and larvae were
713 fixed and analyzed at 14dpt.
714 **B)** Whole mount fluorescent immunohistochemistry (GFP and mCherry) of the pancreas of
715 *Tg(hsp70:CaN^{CA}); Tg(ins:NTR-P2A-mCherry); Tg(nkx6.1:GFP)* larvae at 14dpt. 3D projection
716 (stack) of one non-ablated and one ablated with or without heat-shock representative
717 samples. The principal islet (PI) and the pancreatic tail are showed. Arrows point out mCherry+
718 beta cells in the pancreatic tail. Scale 100µM.
719 **C)** Barplot representing the mean number of mCherry+ beta cells in the pancreatic tail of
720 *Tg(hsp70:CaN^{CA}); Tg(ins:NTR-P2A-mCherry); Tg(nkx6.1:GFP)* larvae at 14dpt. The gray spheres
721 represent non-ablated condition ; the pink triangles represent the ablated condition ; the black
722 squares heat-shock condition and inverted green triangles ablated + heat-shock condition.
723 Data are presented as mean values ± SD. Two-way ANOVA with Tukey's multiple comparisons
724 test, *p-value<0.05, *** p-value<0.0005, ns = non-significant.
725 **D)** Whole mount fluorescent immunohistochemistry (GFP and mCherry) of the pancreas of larvae
726 at 14dpt. 3D projection (stack) of *Tg(ins:NTR-P2A-mCherry) ; Tg(nkx6.1:GFP)* one non-ablated
727 and one ablated representative control samples and *Tg(UAS:CaN^{CA}); Tg(ins:NTR-P2A-mCherry)*
728 *; Tg(cftr:gal4)* one non-ablated and one ablated representative samples. The principal islet (PI)
729 and the pancreatic tail are showed. Arrows point out mCherry+ beta cells in the pancreatic tail.
730 Scale 100µM.
731 **E)** Barplot representing the mean number of mCherry+ beta cells in the pancreatic tail of larvae
732 at 14dpt. The gray spheres represent non-ablated *Tg(ins:NTR-P2A-mCherry) ; Tg(nkx6.1:GFP)*
733 condition ; the pink triangles represent the ablated *Tg(ins:NTR-P2A-mCherry) ; Tg(nkx6.1:GFP)*
734 condition ; the black squares non-ablated *Tg(UAS:CaN^{CA}); Tg(ins:NTR-P2A-mCherry) ;*
735 *Tg(cftr:gal4)* condition and inverted green triangles ablated *Tg(UAS:CaN^{CA}); Tg(ins:NTR-P2A-*
736 *mCherry) ; Tg(cftr:gal4)* condition. Data are presented as mean values ± SD. Two-way ANOVA
737 with Tukey's multiple comparison test, *** means p-value<0.0005, **** p-value<0.00005, ns
738 = non-significant.

739 **Figure 4:** *CaN repression potentializes the effect of Notch inhibition on beta cell formation*

740 **A)** Experimental design for Notch inhibition test in non-ablated condition. Larvae were treated
741 concomitantly with LY411575 (Notch inhibitor) and CsA from 3 to 4dpf and were fixed and
742 analyzed at 6dpf.
743 **B)** Graph representing the mean number of mCherry+ beta cells in the pancreatic tail of
744 *Tg(ins:NTR-P2A-mCherry) ; Tg(nkx6.1:GFP)* larvae at 6 dpf depending the concentration of
745 LY411575. The blue dots represent LY411575; and purple combination of LY411575 and CsA.
746 Data are presented as mean values ± SEM. Two-way ANOVA test with Sidak's multiple
747 comparison test, *p-value<0.05, **p-value<0.05, ns = non-significant.
748 **C)** Whole mount fluorescent immunohistochemistry (GFP and mCherry) of the pancreas of
749 *Tg(ins:NTR-P2A-mCherry) ; Tg(nkx6.1:GFP)* larvae at 6dpf. 3D projection (stack) of one control
750 (without any treatment) ; one CsA-treated ; one LY411757-treated and one with both CsA and
751 LY411575 treated larvae. The principal islet (PI) and the pancreatic tail are showed. Arrows
752 point out mCherry+ beta cells in the pancreatic tail. Scale 50µM.
753 **D)** Barplot representing the mean number of mCherry+ beta cells in the pancreatic tail of
754 *Tg(ins:NTR-P2A-mCherry) ; Tg(nkx6.1:GFP)* larvae at 6dpf. The black dots represent the
755 control; gray CsA treatment ;blue LY411575; and purple combination of LY411575 and CsA.

Data are presented as mean values ± SD. Two-way ANOVA with Tukey multiple comparison test, ***p-value<0.0005, ****p-value<0.00005.

E) Graph representing the mean number of mCherry+ beta cells in the pancreatic tail of *Tg(ins:NTR-P2A-mCherry) ; Tg(nkx6.1:GFP)* larvae at 5-6-7 dpf. The black dots represent the control; gray CsA treatment ;blue LY411575; and purple combination of LY411575 and CsA. Data are presented as mean values ± SEM. Two-way ANOVA test with Sidak's multiple comparison test, *p-value<0.05.

<u>Figure 5:</u> *CaN repression increases the proportion of ductal proliferating cells*

A) Experimental design for EdU assay in Notch test. Larvae were treated concomitantly with LY411575 (Notch inhibitor) and CsA from 3 to 4dpf and then briefly treated with EdU before fixation and analysis at 4 dpf or at 6dpf.

B) Whole mount fluorescent immunohistochemistry (GFP and EdU) of the pancreatic tail of *Tg(ins:NTR-P2A-mCherry) ; Tg(nkx6.1:GFP)* larvae at 4dpf. 3D projection (stack) of one control (without any treatment), one with CsA only, one with LY411575 only and one with both CsA and LY411757 representative samples. Scale 50µM.

C) Barplot representing the percentage of GFP+ ductal cells which incorporated EdU+ in pancreatic tail of *Tg(ins:NTR-P2A-mCherry) ; Tg(nkx6.1:GFP)* larvae for the Notch test. The black dots represent the control; gray CsA treatment ;blue LY411575; and purple combination of LY411575 and CsA. Data are presented as mean values ± SD. T-test. Two-way ANOVA test with Tukey's multiple comparisons test, *p-value<0.05 ; ****p-value<0.00005 ; ns = non-significant.

D) Barplot representing the number of GFP+ ductal cells which in pancreatic tail of *Tg(ins:NTR-P2A-mCherry) ; Tg(nkx6.1:GFP)* larvae at 6dpf for the Notch test. The black dots represent the control; gray CsA treatment ;blue LY411575; and purple combination of LY411575 and CsA. Data are presented as mean values ± SD. T-test. Two-way ANOVA test with Tukey's multiple comparisons test, *p-value<0.05 ; ****p-value<0.00005 ; ns = non-significant.

E) Experimental design for EdU assay in regeneration. Larvae were treated with nifurpirinol for beta cell ablation from 3 to 4dpf then with CsA from 4 to 5dpf and then briefly treated with EdU before fixation and analysis.

F) Whole mount fluorescent immunohistochemistry (GFP and EdU) of the pancreatic tail of *Tg(ins:NTR-P2A-mCherry) ; Tg(nkx6.1:GFP)* larvae at 5dpf. 3D projection (stack) of one representative sample of non-ablated or ablated with or without CsA are shown. Scale 50µM.

G) Barplot representing the percentage of GFP+ ductal cells which incorporated EdU+ in pancreatic tail of *Tg(ins:NTR-P2A-mCherry) ; Tg(nkx6.1:GFP)* larvae at 5dpf. The gray spheres represent non-ablated condition ; the pink triangles the ablated condition ; the black squares CsA condition and inverted green triangles ablated + CsA condition. Data are presented as mean values ± SD. Two-way ANOVA test with Tukey's multiple comparisons test, *p-value<0.05 ; ****p-value<0.00005 ; ns = non-significant.

H) Whole mount fluorescent immunohistochemistry (VenusPest and EdU) of the pancreatic tail of *Tg(ins:NTR-P2A-mCherry) ; Tg(tp1:VenusPest)* larvae at 5dpf. 3D projection (stack) of one representative sample of non-ablated or ablated with or without CsA are shown. Scale 50µM.

I) Barplot representing the percentage of GFP+ ductal cells which incorporated EdU+ in pancreatic tail of *Tg(ins:NTR-P2A-mCherry) ; Tg(tp1:VenusPest)* larvae at 5dpf. The gray spheres represent non-ablated condition ; the pink triangles the ablated condition ; the black squares CsA condition and inverted green triangles ablated + CsA condition. Data are presented as mean values ± sd. Two-way ANOVA test with Tukey multiple comparisons test, *p-value<0.05 ; ****p-value<0.00005 ; ns means non-significant.

803 **J)** Barplot representing the number of VenusPest+ ductal cells which incorporated EdU+ in
804 pancreatic tail of *Tg(ins:NTR-P2A-mCherry) ; Tg(tp1:VenusPest)* larvae at 5dpf. The gray
805 spheres represent non-ablated condition ; the pink triangles the ablated condition ; the black
806 squares CsA condition and inverted green triangles ablated + CsA condition. Data are
807 presented as mean values ± SD. Two-way ANOVA test with Tukey's multiple comparisons test,
808 **p-value<0.005.
809

810 **Figure 6:** *CaN regulation is important in juveniles/adults and necessary for correct glycemia recovery*

811 **A)** Whole mount fluorescent immunohistochemistry (GFP and mCherry) of the pancreas of
812 *Tg(ins:NTR-P2A-mCherry) ; Tg(nkx6.1:GFP)* 2 months old zebrafish at 7dpt. 3D projection (stack)
813 of non-ablated and ablated larvae treated with DMSO or CsA representative samples. The
814 principal islet (PI) and the pancreatic tail are shown. Zoom from section of the pancreatic tail
815 are shown, arrows point out mCherry+ beta cells in these zoom. Scale 200µM

816 **B-C)** Barplot representing the number of number of mCherry+ small secondary islets (=<5 cells) in
817 the pancreatic tail of *Tg(ins:NTR-P2A-mCherry) ; Tg(nkx6.1:GFP)* 2 months old zebrafish at 7 **(B)** and
818 10dpt **(C).** The gray spheres represent non-ablated condition ; the pink triangles represent the
819 ablated condition ; the black squares CsA condition and inverted green triangles ablated + CsA
820 condition. Data are presented as mean values ± SD. Two-way ANOVA with Tukey's multiple
821 comparison test, *p-value<0.05.

822

823 **D-E)** Barplot representing the glycemia (mg/dL) of *Tg(ins:NTR-P2A-mCherry) ;* months old adult
824 zebrafish at 7 **(D)** and 10dpt **(E).** The pink triangles represent the ablated condition ; the inverted
825 green triangles ablated + CsA condition; the blue squares *Tg(hsp70:CaN^{CA})* after heat shocks ; the
826 orange lozenges *Tg(UAS:CaN^{CA})*; *Tg(cftr:gal4)*. The grey line represents the mean glycemia of
827 controls (non-ablated) fish. Data are presented as mean values ± SD. One-way ANOVA with Tukey's
828 multiple comparison test, *p-value<0.05; **p-value<0.005.

829

830 **Figure 7:** *Model of CaN action on ductal progenitors to regenerate beta cells*

831 **A)** Under physiological conditions, the behavior of the ductal progenitors is determined by
832 Notch signaling. Calcineurin is active in these progenitors and enable a proper control
833 between proliferation and differentiation. When CaN in repressed, more ductal
834 progenitors enter in the cell cycle (2dpt) and switch to a mode of proliferation leading to
835 differentiation of the two daughter cells (4dpt), as more pro-endocrine cells are formed.
836 The result is a exhaustion of the progenitors and a premature beta cell differentiation
837 (10dpt).

838

839 **Figure 1 supplemental :** *Transcriptomic profiling of ductal cells during beta cell regeneration and*
840 *validation in larvae*

841 A) Design of the experimental pipeline for transcriptomic experiment

842 B) Expression of *ppp3cca; ppp3ccb ; nfatc3a ; nfatc3b* in acinar, alpha, beta, delta or ductal cells
843 population from the zebrafish pancreas [40].

844 C) Calcineurin (*ppp3ccb and ppp3cca)* and NFATc3 (*nfatc3a and nfatc3b)* expression in ductal cells
845 from zebrafish in non-ablated and ablated conditions.

846 **Figure 2 supplemental :** *Calcineurin inhibition with CsA increases the ductal regenerative response*

847 **A)** Whole mount fluorescent immunohistochemistry (mCherry) of the pancreas of *Tg(ins:NTR-*
848 *P2A-mCherry)* larvae at 4-7 and 14dpt. 3D projection (stack) of ablated larvae treated with
849 DMSO or CsA representative samples. The principal islet (PI) and the pancreatic tail are shown.
850 Scale 50 or 100µM.

851 **B-C)** Barplot representing the number of mCherry+ beta cells in the principal islet (PI) **(B)** and the
852 number of secondary islets of mCherry+ beta cells in the pancreatic tail **(C)** of Tg(ins:NTR-P2A-
853 mCherry) ; Tg(nkx6.1:GFP) larvae at 10dpt. Data are presented as mean values ± SD. T-test or
854 Two-way ANOVA with Tukey's multiple comparison test. **p-value<0.005

855 **D)** Barplot representing the number of sst1.1+ mCherry+ bi-hormonal cells in the principal islet
856 (PI) of Tg(ins:NTR-P2A-mCherry) ; Tg(sst1.1:GFP) larvae at 6dpt. Data are presented as mean
857 values ± SD. T-test.

858 **E)** Experimental design for EdU assay in larvae. After NFP treatment for 3 to 4dpf, larvae were
859 exposed to EdU before fixation for analysis.

860 **F)** Whole mount fluorescent immunohistochemistry (GFP and EdU) of the pancreas of
861 Tg(ins:NTR-P2A-mCherry) ; Tg(neurod1:GFP) larvae at 2-4-7 and 10 dpt. 3D projection (stack) of
862 non-ablated and ablated larvae treated with DMSO or CsA representative samples. The principal
863 islet (PI) and the pancreatic tail are shown. Scale 50µM.

864 **G-H)** Barplot representing the number of gcg+ alpha cells **(G)**; the number of GFP+ sst1.1 delta
865 cells **(H);** of Tg(*ins:NTR-P2A-mCherry*) ; Tg(*sst1.1:GFP*) larvae at 10dpt. Gcg was detected by IHC.
866 The gray spheres represent non-ablated condition ; the pink triangles represent the ablated
867 condition ; the black squares CsA condition and inverted green triangles ablated + CsA condition.
868 Data are presented as mean values ± SD. Two-way ANOVA with Tukey's multiple comparison
869 test. **p-value<0.005

870

871 **Figure 4 supplemental :** *CaN repression potentializes the effect of Notch inhibition on beta cell*
872 *formation*

873 **A)** Experimental design for Notch inhibition test in non-ablated condition. Larvae were treated
874 concomitantly with LY411575 (Notch inhibitor) and FK506 from 3 to 4dpf and were fixed and
875 analyzed at 5dpf.
876 **B)** Barplot representing the mean number of mCherry+ beta cells in the pancreatic tail of
877 *Tg(ins:NTR-P2A-mCherry) ; Tg(nkx6.1:GFP)* larvae at 5dpf. The black dots represent the control;
878 gray FK506 treatment ;blue LY411575; and purple combination of LY411575 and FK506. Data
879 are presented as mean values ± SD. Two-way ANOVA with Tukey multiple comparison test,
880 *p-value<0.05,**p-value<0.005, ****p-value<0.00005.
881 **C)** Experimental design for Notch inhibition test in non-ablated condition. Larvae were heat-
882 shocked and then directly treated with LY411575 (Notch inhibitor) from 3 to 4dpf and were
883 fixed and analyzed at 6dpf.
884 **D)** Barplot representing the mean number of mCherry+ beta cells in the pancreatic tail of
885 *Tg(hsp70:CaN^{CA})*; *Tg(ins:NTR-P2A-mCherry) ; Tg(nkx6.1:GFP)* larvae at 5dpf. The black dots

886 represent the control; gray heat-shock ;blue LY411575; and purple combination of LY411575
887 and heat-shock. Data are presented as mean values ± SD. Two-way ANOVA with Tukey multiple
888 comparison test, ****p-value<0.00005.
889 **E)** Barplot representing the mean number of mCherry+ beta cells in the pancreatic tail of
890 *Tg(ins:NTR-P2A-mCherry) ; Tg(nkx6.1:GFP)* larvae at 6dpf after Notch inhibition (LY411575),
891 CaN inhibition (CsA) and NFATc inhibition (CHIR99021). Data are presented as mean values ±
892 SD. Two-way ANOVA with Tukey multiple comparison test, *p-value<0.05,**p-value<0.005,
893 ****p-value<0.00005.
894

895 **Figure 5 supplemental:** *CaN repression increases the proportion of duct proliferating cells*

896 **A-C)** Barplot representing the number of GFP+ ductal cells which in pancreatic tail of *Tg(ins:NTR-*
897 *P2A-mCherry) ; Tg(nkx6.1:GFP)* larvae at 4dpf for the Notch test. **(B)** Mild Notch inhibition with
898 LY411575 5µM and **(C)** stronger Notch inhibition with LY411575 15µM. The black dots represent
899 the control; gray CsA treatment ;blue LY411575; and purple combination of LY411575 and CsA.
900 Data are presented as mean values ± SD. T-test. Two-way ANOVA test with Tukey's multiple
901 comparisons test, *p-value<0.05 ; ****p-value<0.00005 ; ns = non-significant.

902 **B)** Z-plan pictures of Tg (nkx6.1:GFP); Tg (ins:NTR*-mCherry) larvae that were treated at 3dpf with
903 both CsA 1µM and LY411575 5µM. At 4dpf, the larvae were exposed to EdU 4mM during 8
904 hours, before analysis at 6 dpf.

905

906 **Figure 6 supplemental:** *CaN regulation is important in juveniles/adults and necessary for correct*
907 *glycemia recovery*

908 **A)** Barplot representing the glycemia (mg/dL) of *Tg(ins:NTR-P2A-mCherry) ;* months old adult
909 zebrafish at 14dpt**.** The pink triangles represent the ablated condition ; the inverted green
910 triangles ablated + CsA condition; the blue squares *Tg(hsp70:CaN^{CA}*) after heat shocks. The
911 grey line represents the mean glycemia of controls (non-ablated) fish. Data are presented as
912 mean values ± SD.
913 **B)** Barplot representing the glycemia (mg/dL) of *Tg(ins:NTR-P2A-mCherry) ; and Tg(UAS:CaN^{CA}*);
914 *Tg(cftr:gal4)* in non-ablated adult zebrafish. Data are presented as mean values ± SD.

915

916

917

918

919

920

921

922

923

924

Figure 1

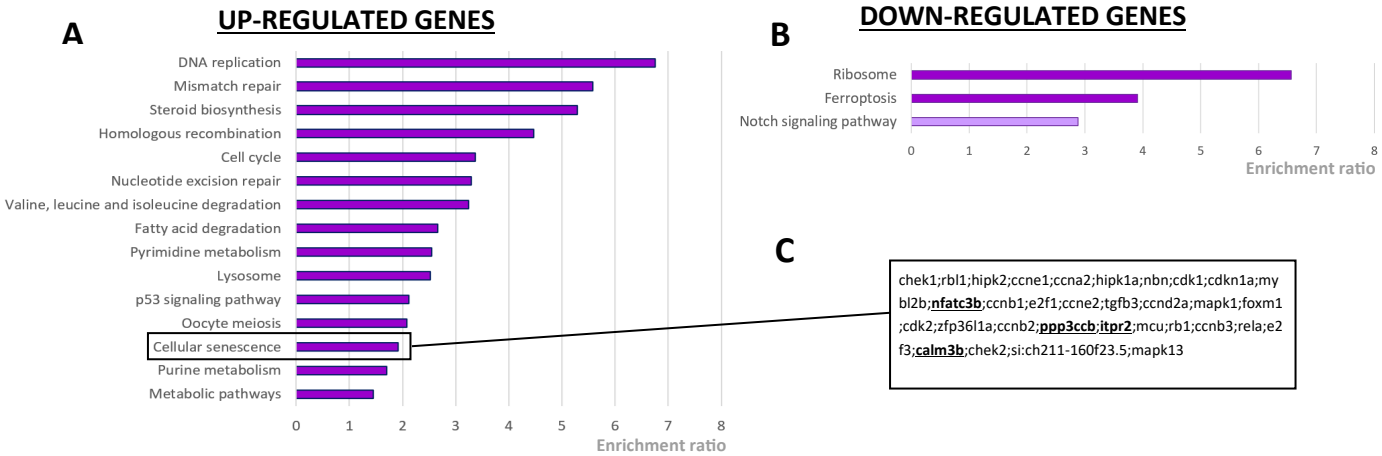
A
UP-REGULATED GENES
DNA replication
Mismatch repair
Steroid biosynthesis
Homologous recombination
Cell cycle
Nucleotide excision repair
Valine, leucine and isoleucine degradation
Fatty acid degradation
Pyrimidine metabolism
Lysosome
p53 signaling pathway
Oocyte meiosis
Cellular senescence
Purine metabolism
Metabolic pathways
0 1 2 3 4 5 6 7 8
Enrichment ratio
B
DOWN-REGULATED GENES
Ribosome
Ferroptosis
Notch signaling pathway
0 1 2 3 4 5 6 7 8
Enrichment ratio
C
chek1;rbl1;hipk2;ccne1;ccna2;hipk1a;nbn;cdk1;cdkn1a;mybl2b;nfatc3b;ccnb1;e2f1;ccne2;tgfb3;ccnd2a;mapk1;foxm1;cdk2;zfp36l1a;ccnb2;ppp3ccb;itpr2;mcu;rb1;ccnb3;rela;e2f3;calm3b;chek2;si:ch211-160f23.5;mapk13

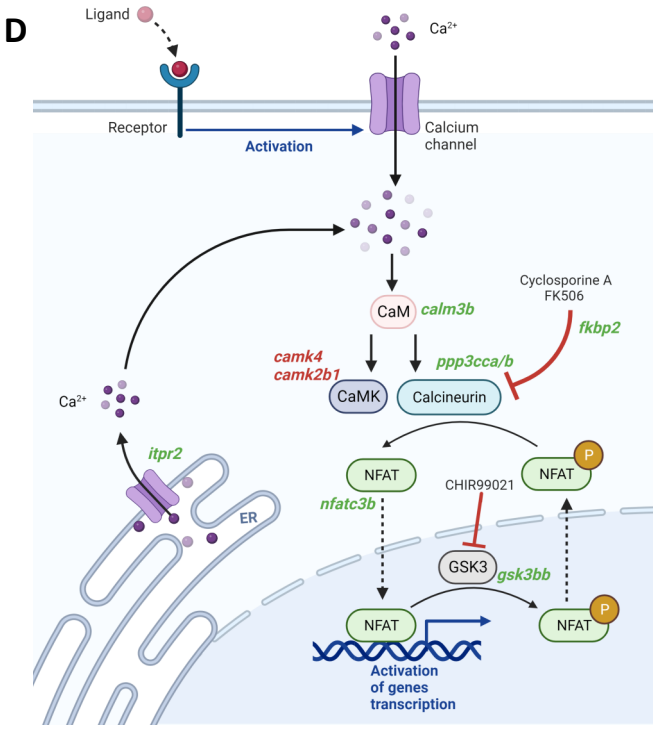
D
Ligand
Ca2+
Receptor
Activation
Calcium channel
Cyclosporine A
FK506
CaM
calm3b
fkbp2
camk4
camk2b1
ppp3cca/b
CaMK
Calcineurin
Ca2+
itpr2
ER
NFAT
P
CHIR99021
nfatc3b
GSK3
gsk3bb
Activation of genes transcription

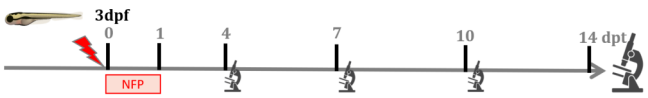
E
3dpf
0
1
4
7
10
14 dpt
NFP

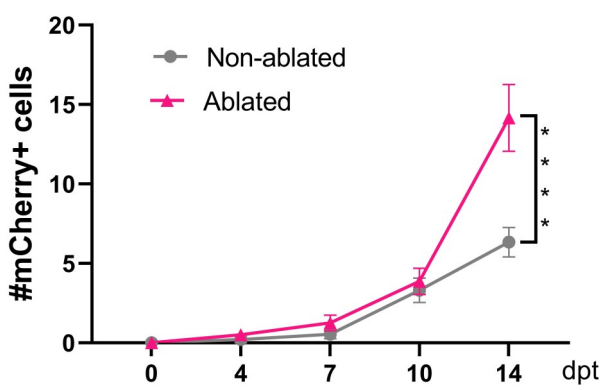
F
#mCherry+ cells
Non-ablated
Ablated
0
5
10
15
20
0
4
7
10
14
dpt
*
*
*
*

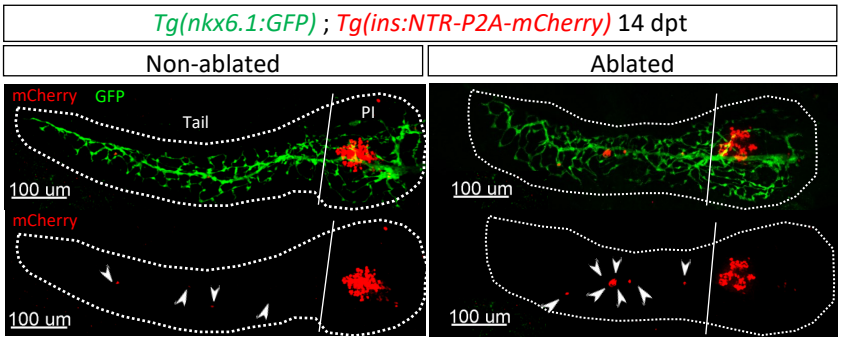
G
Tg(nkx6.1:GFP) ; Tg(ins:NTR-P2A-mCherry) 14 dpt
Non-ablated
Ablated
mCherry GFP
Tail
PI
100 um
mCherry
100 um
100 um
100 um

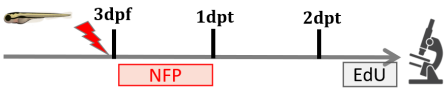
H
3dpf
1dpt
2dpt
NFP
EdU

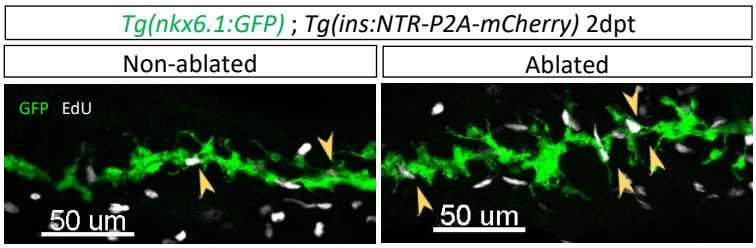
I
Tg(nkx6.1:GFP) ; Tg(ins:NTR-P2A-mCherry) 2dpt
Non-ablated
Ablated
GFP EdU
50 um
50 um

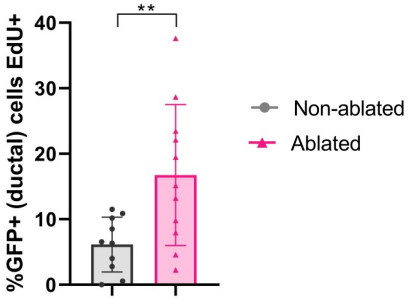
J
%GFP+ (ductal) cells EdU+
0
10
20
30
40
**
Non-ablated
Ablated

Figure 2

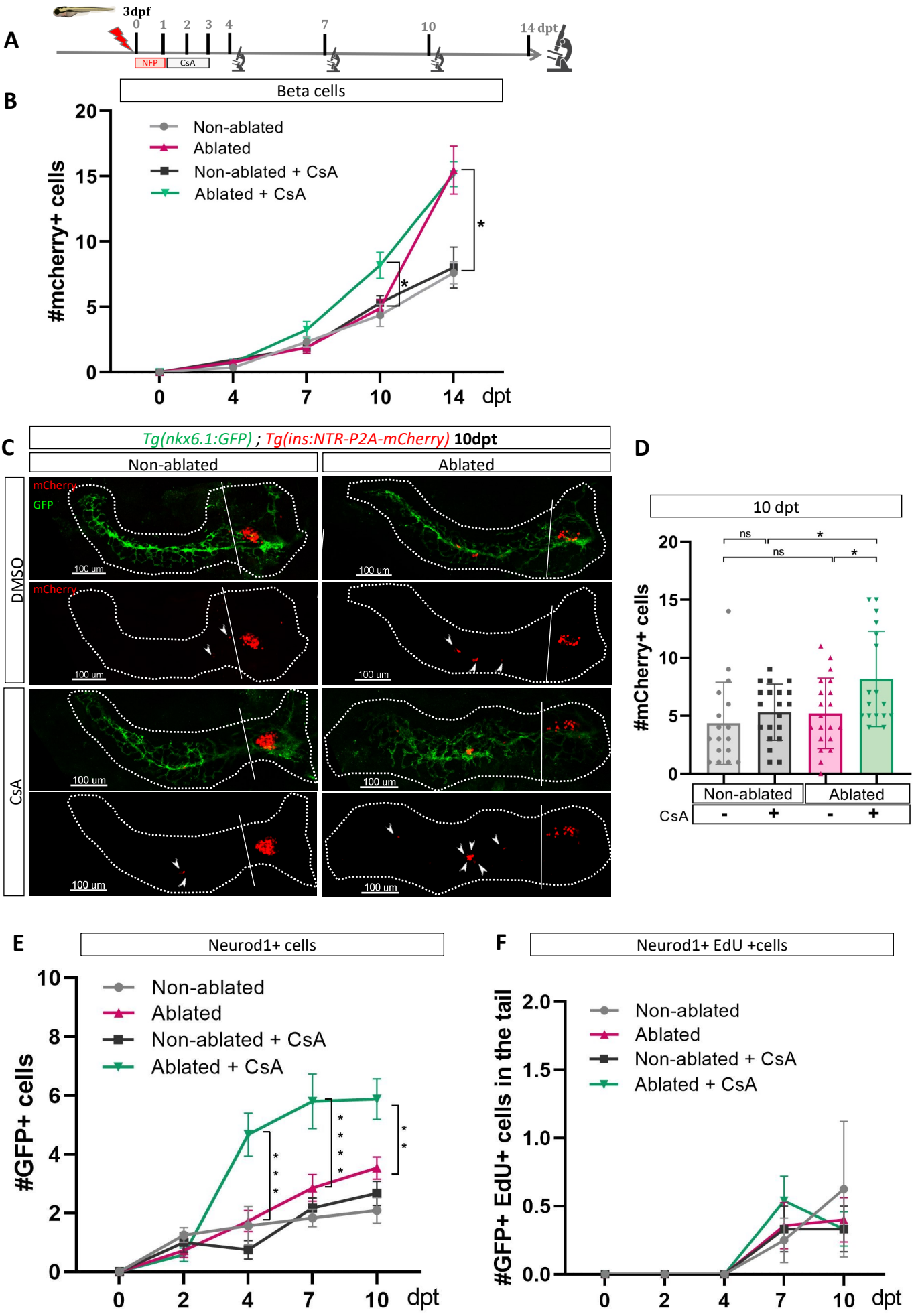
A
3dpf
0
1
2
3
4
7
10
14 dpt
NFP
CsA
B
Beta cells
#mcherry+ cells
Non-ablated
Ablated
Non-ablated + CsA
Ablated + CsA
dpt
C
Tg(nkx6.1:GFP) ; Tg(ins:NTR-P2A-mCherry) 10dpt
Non-ablated
Ablated
DMSO
CsA
mCherry
GFP
100 um
D
10 dpt
#mCherry+ cells
ns
Non-ablated
Ablated
CsA
E
Neurod1+ cells
#GFP+ cells
Non-ablated
Ablated
Non-ablated + CsA
Ablated + CsA
dpt
F
Neurod1+ EdU +cells
#GFP+ EdU+ cells in the tail
Non-ablated
Ablated
Non-ablated + CsA
Ablated + CsA
dpt

Figure 3

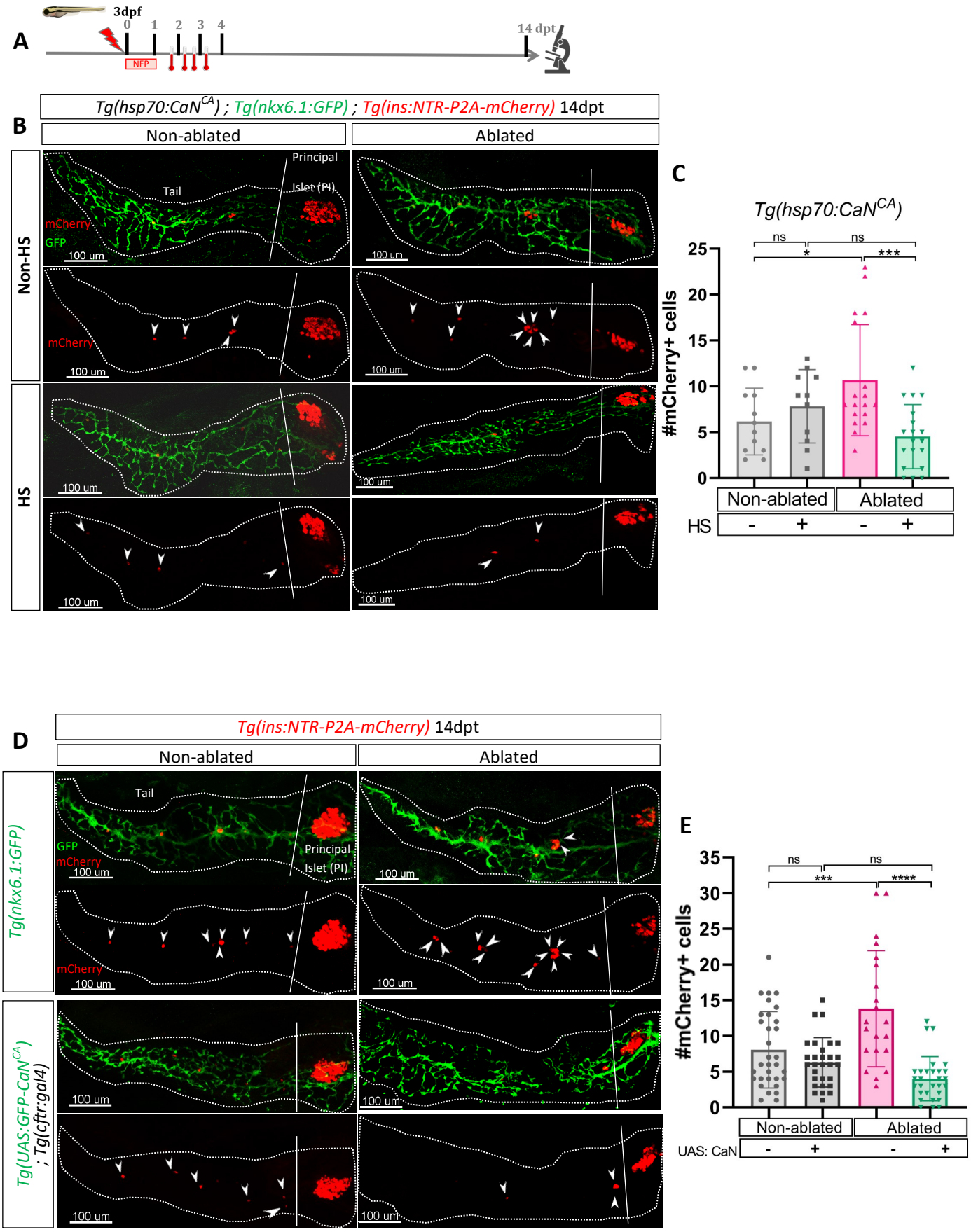
A
3dpf
0
1
2
3
4
NFP
14 dpt
B
Tg(hsp70:CaN^CA) ; Tg(nkx6.1:GFP) ; Tg(ins:NTR-P2A-mCherry) 14dpt
Non-ablated
Ablated
Non-HS
HS
Tail
Principal Islet (PI)
mCherry
GFP
100 um
C
Tg(hsp70:CaN^CA)
#mCherry+ cells
ns
ns
*
***
Non-ablated
Ablated
HS
-
+
-
+
D
Tg(ins:NTR-P2A-mCherry) 14dpt
Non-ablated
Ablated
Tg(nkx6.1:GFP)
Tg(UAS:GFP-CaN^CA) ; Tg(cftr:gal4)
Tail
Principal Islet (PI)
GFP
mCherry
100 um
E
#mCherry+ cells
ns
ns
***
****
Non-ablated
Ablated
UAS: CaN
-
+
-
+

Figure 4

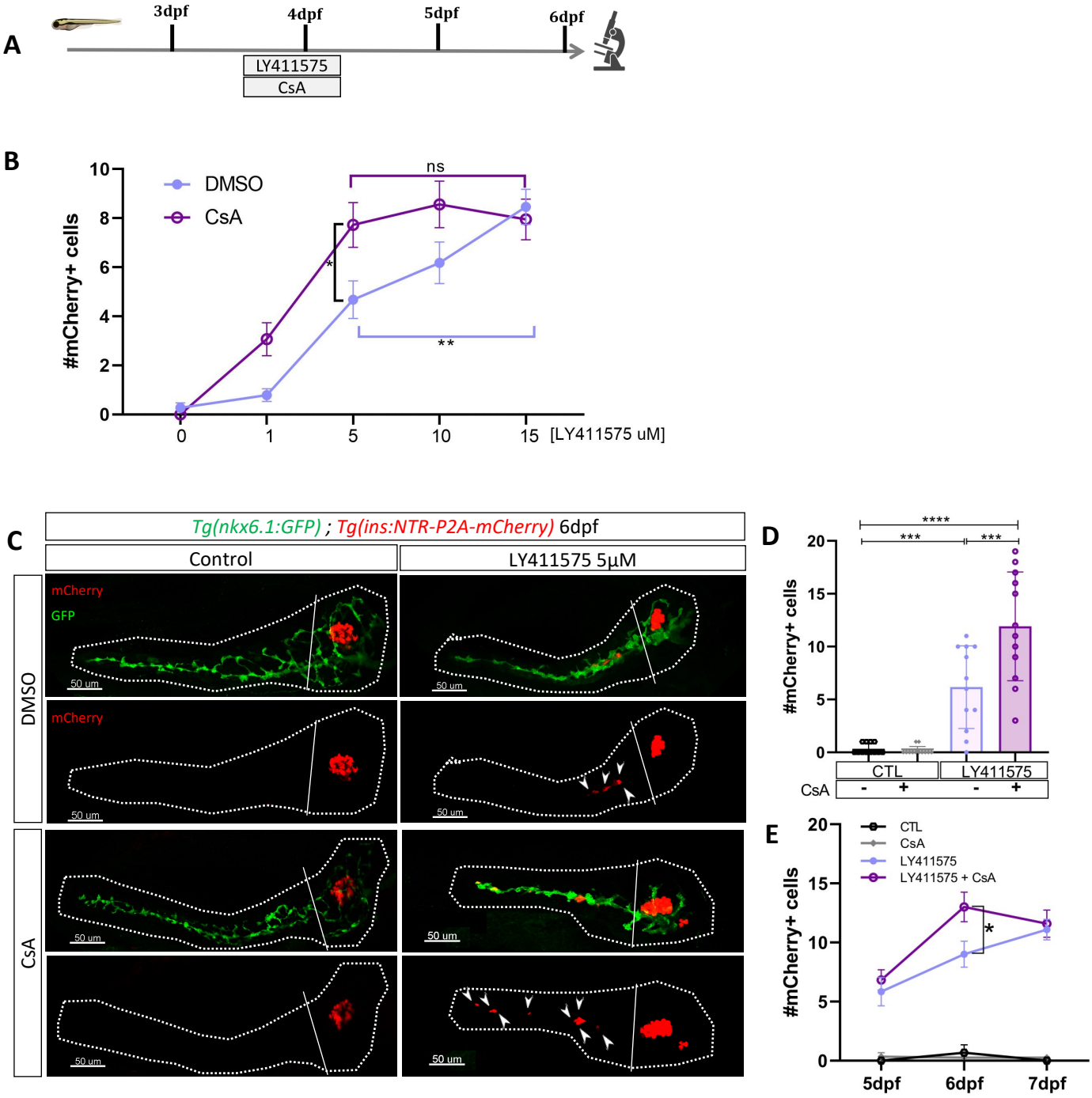
A
3dpf
4dpf
5dpf
6dpf
LY411575
CsA
B
DMSO
CsA
ns
*
**
#mCherry+ cells
[LY411575 uM]
C
Tg(nkx6.1:GFP) ; Tg(ins:NTR-P2A-mCherry) 6dpf
Control
LY411575 5µM
DMSO
CsA
mCherry
GFP
50 um
D
****
***
***
#mCherry+ cells
CTL
LY411575
CsA
E
CTL
CsA
LY411575
LY411575 + CsA
#mCherry+ cells
5dpf
6dpf
7dpf

Figure 5

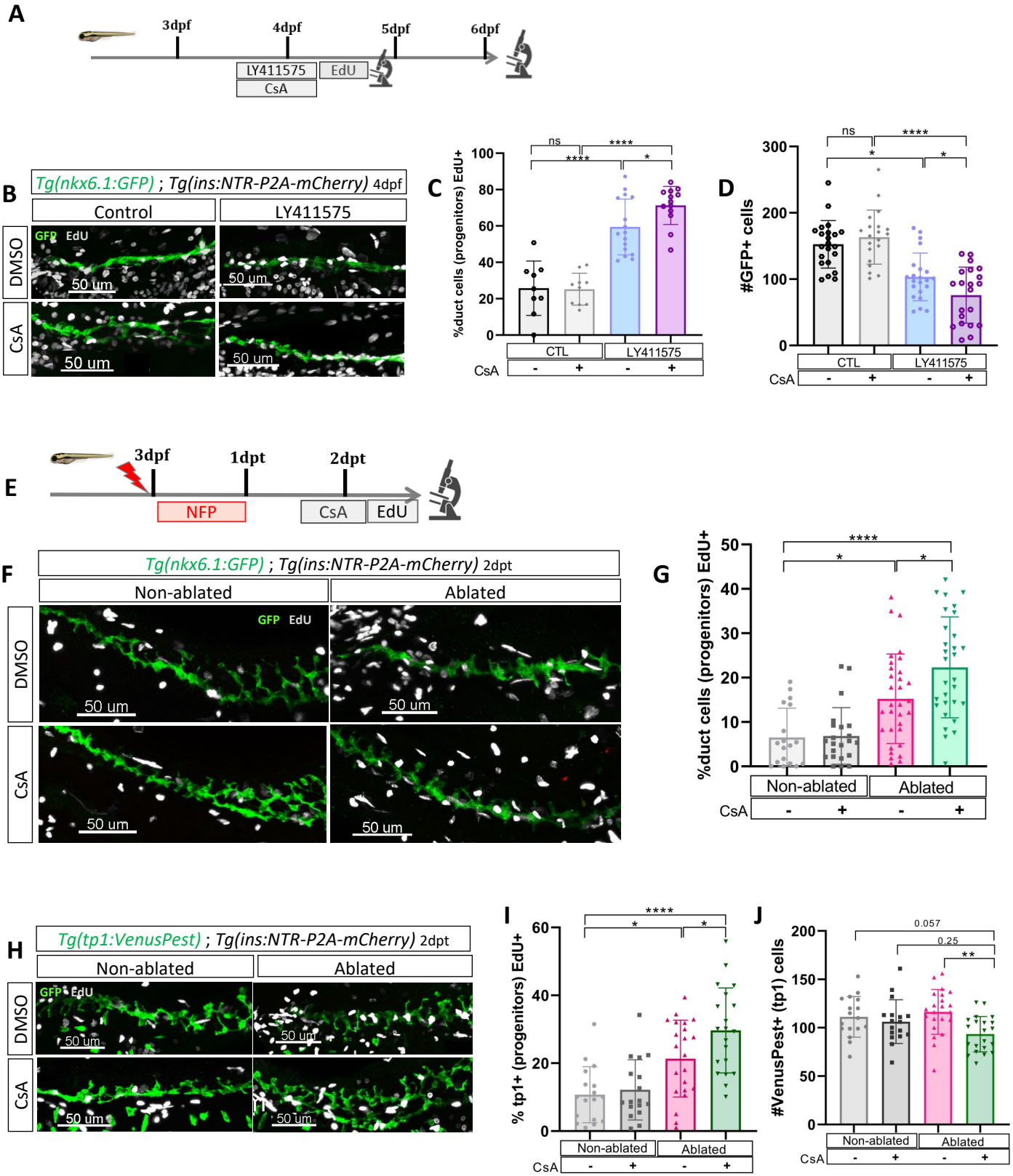
A
3dpf
4dpf
5dpf
6dpf
LY411575
CsA
EdU
B
Tg(nkx6.1:GFP) ; Tg(ins:NTR-P2A-mCherry) 4dpf
Control
LY411575
DMSO
CsA
GFP EdU
50 um
C
%duct cells (progenitors) EdU+
ns
****
*
CTL
LY411575
CsA
D
#GFP+ cells
E
3dpf
1dpt
2dpt
NFP
CsA
EdU
F
Tg(nkx6.1:GFP) ; Tg(ins:NTR-P2A-mCherry) 2dpt
Non-ablated
Ablated
G
%duct cells (progenitors) EdU+
H
Tg(tp1:VenusPest) ; Tg(ins:NTR-P2A-mCherry) 2dpt
I
% tp1+ (progenitors) EdU+
J
#VenusPest+ (tp1) cells
0.057
0.25
**

Figure 6

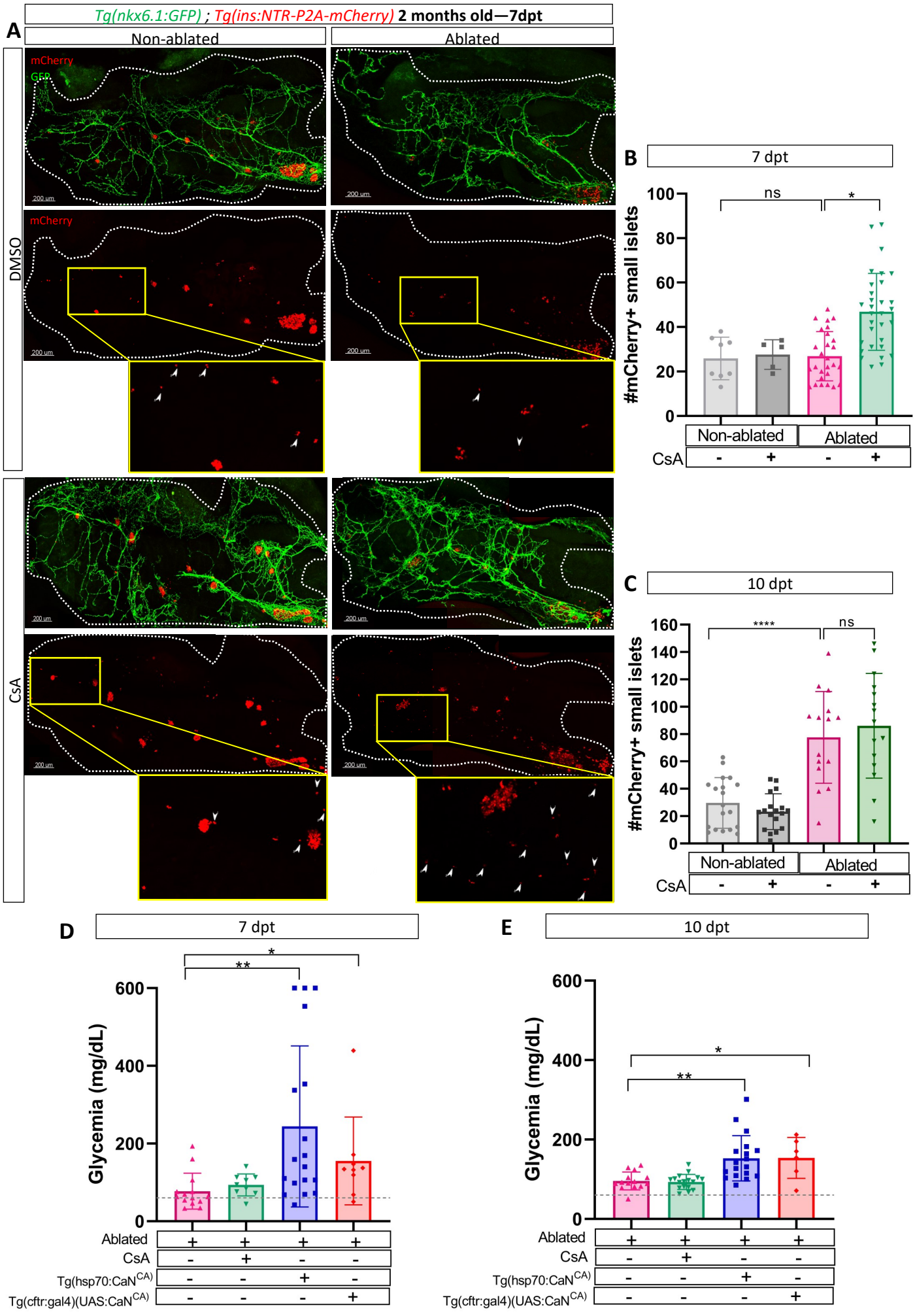
A
Tg(nkx6.1:GFP) ; Tg(ins:NTR-P2A-mCherry) 2 months old—7dpt
Non-ablated
Ablated
mCherry
GFP
DMSO
CsA
200 um
B
7 dpt
#mCherry+ small islets
ns
*
Non-ablated
Ablated
CsA
C
10 dpt
****
ns
D
7 dpt
Glycemia (mg/dL)
Ablated
CsA
Tg(hsp70:CaN^CA)
Tg(cftr:gal4)(UAS:CaN^CA)
E
10 dpt

Figure 7

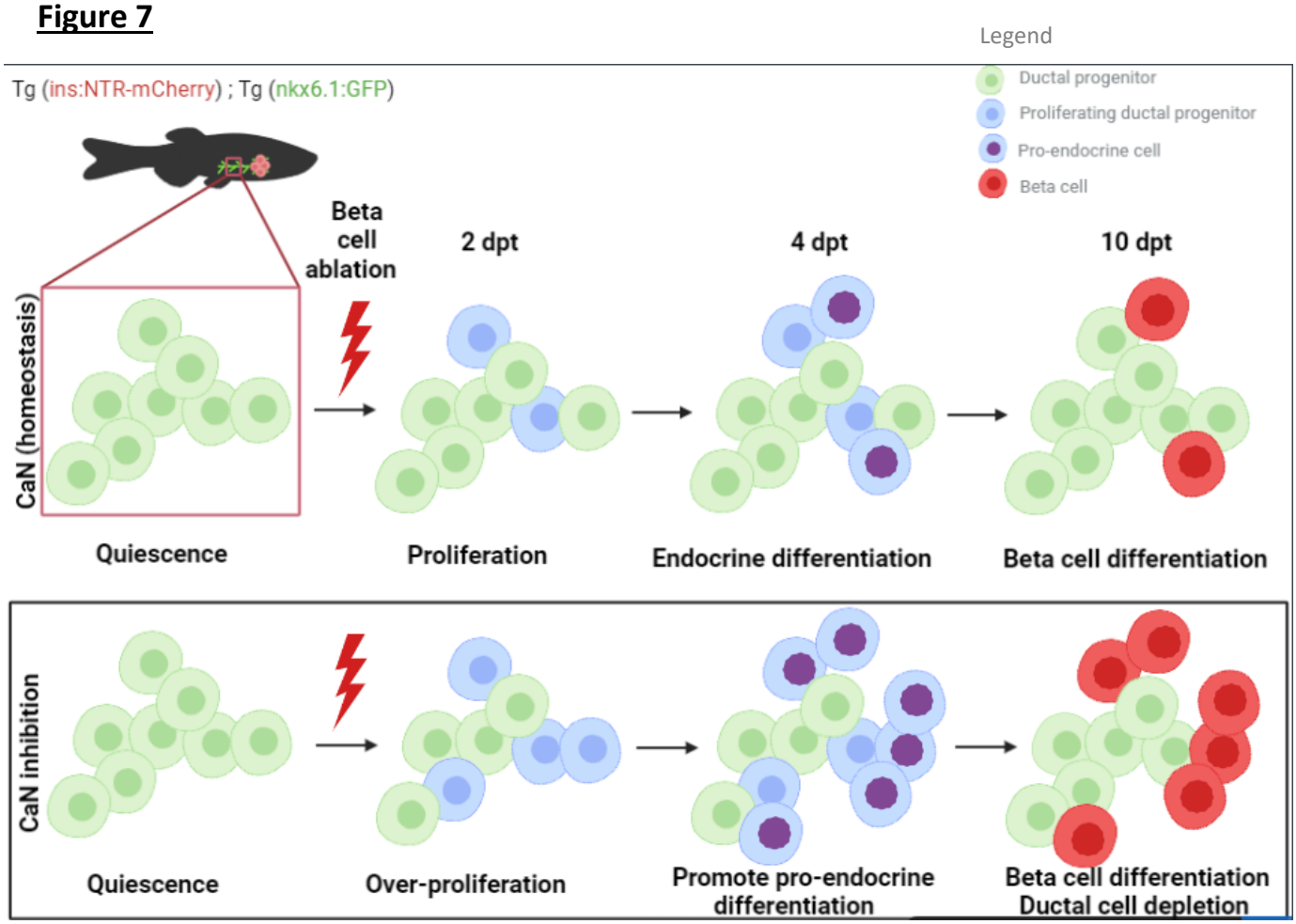
Legend
Ductal progenitor
Proliferating ductal progenitor
Pro-endocrine cell
Beta cell
Tg (ins:NTR-mCherry) ; Tg (nkx6.1:GFP)
Beta cell ablation
2 dpt
4 dpt
10 dpt
CaN (homeostasis)
Quiescence
Proliferation
Endocrine differentiation
Beta cell differentiation
CaN inhibition
Quiescence
Over-proliferation
Promote pro-endocrine differentiation
Beta cell differentiation
Ductal cell depletion